Article

Not peer-reviewed version

A Novel Battery-Supplied AFE EEG Circuit Capable of Muscle Movement Artifact Suppression

Athanasios Delis *, George Tsavdaridis, Panayiotis Tsanakas

Posted Date: 3 June 2024

doi: 10.20944/preprints202404.2023.v2

Keywords: electroencephalography; EEG; muscle artifacts; notch filter; driving right leg; battery-based EEG signal acquisition system; biosignal filtering; low frequency signal; CMRR

Article

A Novel Battery-Supplied AFE EEG Circuit Capable of Muscle Movement Artifact Suppression

Athanasios Delis *, George Tsavdaridis and Panayiotis Tsanakas

School of Electrical & Computer Engineering, National Technical University of Athens, 9, Iroon Polytechniou Str., 15772 Athens, Greece; gtsav@central.ntua.gr (G.T.); panag@cs.ntua.gr (P.T.)

* Correspondence: athanasiosdelis@mail.ntua.gr

Abstract: In this study, the fundamentals of electroencephalography signals, their categorization into frequency sub-bands, the circuitry used for their acquisition, and the impact of noise interference on signal acquisition are examined. Additionally, design specifications for medical-grade and research-grade EEG circuits and a comprehensive analysis of various analog front-end architectures for electroencephalograph (EEG) circuit design are presented. Three distinct selected case studies are examined in terms of comparative evaluation with generic EEG circuit design templates. Moreover, a novel one-channel battery-supplied EEG analog front-end circuit designed to address the requirements of usage protocols containing strong com-pound muscle movements is introduced. Furthermore, a realistic input signal generator circuit is proposed that models the human body and the Electromagnetic Interference from its surroundings. Experimental simulations are conducted in 50 Hz and 60 Hz electrical grid environments to evaluate the performance of the novel design. The results demonstrate the efficacy of the proposed system, particularly in terms of bandwidth, portability, common mode rejection ratio , gain, suppression of muscle movement artifacts, electrostatic discharge and leakage current protection. Conclusively, the novel design is cost-effective and suitable for both commercial and research single-channel EEG applications. It can be easily incorporated in Brain Computer Interfaces and neurofeedback training systems.

Keywords: electroencephalography; EEG; muscle artifacts; notch filter; driving right leg; battery-based EEG signal acquisition system; biosignal filtering; low frequency signal; CMRR

1. Introduction

1.1. Medical Significance of EEG Signals Acquisition

Electroencephalography, a non-invasive signal acquisition technique in Neuroscience [1], is employed for recording the brain's electrical activity via electrodes placed on the scalp. These captured signals are distinguished by their unique frequency, amplitude, and source location characteristics, playing a pivotal role in the diagnosis and monitoring of neurological disorders such as epilepsy, sleep disturbances, brain tumors, cerebral injuries, etc. The high temporal resolution of the Electroencephalograph (in this study, it is denoted by the abbreviation EEG), in contrast with other neuro-imaging modalities such as fMRI, enables the real-time analysis of brain activity, offering valuable insights into cognitive functions and mental states. As a final point, EEG is instrumental in the advancement of Brain-Computer Interfaces (BCIs) [2], contributing significantly to our comprehension of neural dynamics in both healthy and pathological states by enabling telemonitoring of patients, as well as enabling biomedical engineers to create telekinesis applications and neuro-feedback training BCI Systems [3,4]. In clinical settings and in research, particularly in the domains of neurology and neurosurgery, the precise signal acquisition needs to be as accurate and noise-free as possible to determine the patterns of brainwaves and make diagnostic analysis through EEG [5,6].

The technology that entails EEG is an enormously relevant tool in neurological assessments [7], whereby an evaluation and assessment of the electrical activity taking place within the brain is done. It helps to identify some kinds of seizures, which helps develop an accurate protocol of treatment.

 doi:10.20944/preprints202404.2023.v2

EEG identifies the patterns of brain waves for different stages of sleep [8]; it is very important in the diagnosis of sleep abnormalities like narcolepsy. In patients with head injury who have fallen into a coma, EEG is of paramount importance in the assessment of brain responsiveness and the quantification of damage [9]. It may be used in the determination of early abnormal loci within the brain, loci which may be reflecting the onset of ailments such as epilepsy, dementia, and Alzheimer's [10,11].

1.2. EEG Signals into Frequency Sub-bands: Comprehensive Categorization

The EEG signals were represented as the linear combination of many frequencies sub-bands in which each of them bores a unique set of brain activity. Normally, delta waves refer to unconsciousness and deep sleep. Theta waves are associated with meditation, creativity, and insomnia, while alpha waves relate to tranquility, relaxation, and reduced concentration. Beta waves are affix to anxiety, concentration, and active, busy, or deep-thinking mental activities. Gamma waves are attributed to higher mental activities that involve more consciousness or perception [12,13]. This classification induces structure and reproducibility when employed in clinical and research settings, and it enables healthcare providers to analyze brains and diagnose disorders more efficiently. A visualization of each wave type can be seen in Figure 1 (for more details for each wave and its implications see Table A.1 in Appendix A) [12–14].

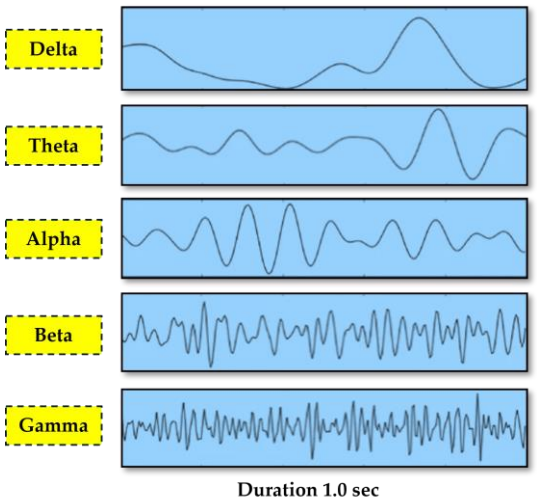

Figure 1. EEG Signals Categorization by Frequency Sub-bands.

1.3. Noise Interference in EEG Signal Acquisition

Noise interference presents a considerable challenge in EEG signal acquisition. It creates noise artifacts that are embedded in the raw EEG data that is collected with electrodes and leads to significant challenges to the interpretation of the real brain's state patterns by practitioners in the fields of Neurology and Neuroscience [15,16]. EEG captures the brain's electrical activity indirectly through scalp electrodes because electrodes capture the voltage fluctuation in the skin that is caused by the projection of an electromagnetic field, causing internal neural activity [17]. Unfortunately, along with the brain's lead field projection in the electrode, the signal that the electrodes capture is also corrupted with unwanted noise artifacts, such as compound muscle movement artifacts, electromagnetic interference, etc. [18]. The purpose of the EEG device is to digitize the least amount of possible noise artifacts that are contained within the original raw EEG signal collected from the electrodes while keeping intact the brain-related component of the raw signal [19,20]. As it becomes apparent from the above, obtaining clear and precise EEG signals is often difficult due to numerous sources of noise interference (for more details for each noise source and their corresponding frequency ranges see Table A.2 in Appendix A) [17,21].

 doi:10.20944/preprints202404.2023.v2

1.4. Design Specifications in Medical-Grade and Research-Grade EEG Generic Circuits Design

In EEG Generic Circuit Design, various subcomponents work together for accurate brainwave signal capturing and denoising. One of the most characteristic examples of them is the Filter subcomponents such as Notch, Anti-Aliasing, High Pass, and Low Pass Filters, which refine signals by eliminating interference and keeping only the frequency bands of interest from the input raw EEG signal [22]. Another example is the Circuit subcomponents, including Chopper Circuits and Electrostatic Discharge Protection (ESD), which minimize low-frequency noise and protect against electrostatic discharge damage. Additionally, the Amplifier subcomponents, such as Operational Amplifiers, Programmable Gain Amplifiers, and Instrumentation Amplifiers, amplify signals with high fidelity [23]. Furthermore, the Analog Multiplexers select signals in multi-channel setups, while the Analog to Digital Converter digitizes the collected signals from the electrodes for further analysis [24]. Moreover, the Drive Right Leg Circuit reduces interference by introducing a feedback loop between the EEG device and the Human Body [22]. Last but not least, the Power Supply subcomponents, such as batteries and regulators, ensure a stable power supply for the device. These integrated subcomponents create a prototypical EEG Generic circuit design for detailed brain activity analysis. The particular order of the subcomponents and the choice of incorporating some of them in the design, along with their multiplicity, are some of the engineering problems of constructing a functional and appropriate EEG device. As it becomes apparent, each engineering decision has trade-offs, that must be well understood for the design to meet its predefined requirements (for more details of the various components involved in EEG circuits, along with their respective functions see Table A.3 in Appendix A).

In the design of circuits for medical-grade and research-grade EEG applications, several essential specifications are critical, and specific requirements should be met. These circuits may have a bandwidth ranging from 0.01 Hz to 20 kHz (maximum frequency application—identifying Directional Hearing Cues), covering a broad spectrum of brain activity pertinent to diverse research and medical requirements [25,26]. In addition to the aforementioned point, managing noise levels is crucial, particularly during the initial stages before the first amplification. It's essential to keep the 0.1 to 10 Hz noise below 1 μVpp [27], and ideally under 0.4 μVpp, to ensure clear signal quality and a high signal-to-noise ratio (SNR) [28]. Furthermore, it must be stated that the EEG signal of interest always appears as an AC differential voltage signal in the raw input EEG data. Consequently, a high Common Mode Rejection Ratio (CMRR) exceeding 90 dB is deemed crucial for filtering out the common components of the input signals that are the major carriers of the noise artifacts and undesirable DC offsets [29]. It's also important to note that compliance with regulations requires ensuring that no more than 10 μA of current returns to the body, along with mandatory ESD protection. [30–32]. The sub-circuits analyzed above are instrumental in achieving signal integrity, thereby ensuring the accuracy and reliability of the data collected. Each design must be tailored to its intended use and optimized for the particular sub-audience that it appeals to in the field of Neuroscience and Medical practice (for more details of the various technical distinctions in design specifications between medical-grade and research-grade EEG circuits see Table A.4 in Appendix A).

1.5. Problem Statement and Structure of the Present Study

The central idea of this study arises from the observation that there is currently a shortage of EEG circuits in recent literature that can simultaneously monitor the theta, alpha, and beta brain wave frequency bands while the user is engaged in usage protocols that involve intense compound muscle movements. As an objective this study aims this study aims to develop a mobile and cost-effective EEG circuit that can acquire accurately the brain signal during usage protocol that need effective handling of muscle artifacts. The proposed system is powered by a battery, uses simple sub-circuits, and incorporates filters to handle muscle artifacts. The system can potentially be used for neuro-feedback training and tele-controlling devices using Brain-Computer Interfaces (BCIs). For purposes of accurate design and reproducibility of this study, a realistic electronic model of the human brain and body is created to simulate the effects of electromagnetic interference (EMI) from the external environment.

 doi:10.20944/preprints202404.2023.v2

The present manuscript is organized as follows:

- Section 1 (Introduction) highlights the medical importance of acquiring an EEG signal and its role in patient monitoring. It also discusses the sub-bands of frequencies into which the EEG signal is classified and introduces the challenges that noise brings in an acquired EEG signal.
- Section 2 (Related Works in EEG Circuit Design Analog Front-End Architectures) discusses design specifications on medical and research-grade EEG circuits. The selected case studies are elaborated with respect to the comparative analysis of various architectures of EEG AFE.
- Section 3 (Materials and Methods: Novel Proposed EEG Analog Front End Circuit System) puts forth a novel methodology for simulating and evaluating the novel EEG AFE circuitry design against practical cases using MATLAB.
- Section 4 (Simulation and Results: Comprehensive Analysis) is presented with the objective to compare the theoretical values with the simulated values in a real-world scenario for the given circuit design EEG-B3V3S7C1. The circuit's performance is simulated into two of the commonest EEG measurement scenarios: the 50Hz and 60Hz power grid environments that exist outside the shielded lab conditions.
- Section 5 (Discussion) discusses the practical implications, potential limitations, and future perspectives of the proposed EEG circuit design.
- Section 6 (Conclusions) summarizes the entire article.
- This study is accompanied by the Appendix A, B, C. Those appendices contain information that are important mostly for a reader that is novice to the field and needs more context and clarification in order to follow the flow of ideas in the main text.

2. Related Works: EEG Circuit Design Analog Front-End Architectures

Modern CMOS technology has greatly favored the development and advancement of the analog front end for EEG applications. [33] Designed using the TSMC 90nm CMOS process, a compact EEG-signal amplifier employing 90nm MOS capacitors has been reported to attain high CMRR and gain but in an area-saving design. Another design [34] used an LNA and HPF with a 3rd-order Butterworth filter to achieve high power efficiency, which is extremely vital for wearable EEG devices. A 4-channel AFE was created in [35] to be versatile in electrode compatibility and also reduce noise. The design in [36] focused on EEG signal acquisition for epilepsy detection. The AFE in [37] provides mode-selectable gains for local field potential and action potential detection. Wireless multi-channel EEG devices [38–40] have not only improved portability and patient comfort but have also shown efficiency and a low power profile through Bluetooth. Some of these innovations include a present-reused DDA AFE [41] and a low-noise chopper instrument amplifier [42]; both designs achieve high CMRR and PSRR, which are important for the acquisition of good EEG signals. Some other works in the field of EEG signal acquisition and monitoring applications include Neonates-Specific EEG System [43], wireless EEG monitoring circuit with compact amplifiers and signal conditioning modules [44], Single-Chip EEG Signal Sampling Circuits [45], and BCI-Specific EEG [46], etc [further details in Appendix B.4].

Following this overview of EEG circuits, a special extended analysis will be conducted on three distinct EEG circuit designs (Case ''1'', ''2'' & ''3''), elaborating on their topology and electronic characteristics. Additionally, specific requirements and specifications essential for efficient EEG signal acquisition for each Case are presented. Finally, simulation and experimental results, and how they could be compared with the EEG Generic Circuit Design are outlined in Appendix B (see Appendices B.1-B.3) in order to validate the efficacy of these circuits, highlighting their potential impact on advancing EEG technology.

2.1. Low-Cost Circuit Design of EEG Analog Front ends: Case ''1''

2.1.1. Description of Topology and Connectivity

The This subsection delineates the topology and connectivity of a cost-effective EEG circuit design, primarily focused on efficient EEG signal amplification and extraction. It incorporates high-

 doi:10.20944/preprints202404.2023.v2

definition graphics (block diagrams and circuit schematics) to depict the design's architecture, offering a clear visual representation of its components and their interconnections. As depicted in Figure 2, the signal is initially boosted in a pre-amplification stage. Subsequently, low-frequency drifts are removed with a high pass filter. Furthermore, electrical interference at 50Hz is eliminated by a notch filter and high-frequency noise is filtered out with a low pass filter. Finally, a post amplification step is used to achieve the final results of enhanced signal integrity [47].

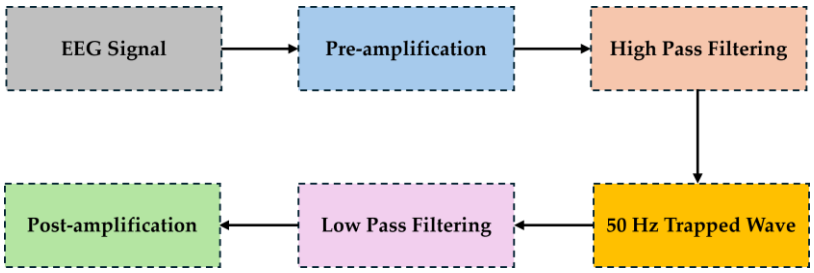

Figure 2. Overall structure of low-cost EEG Circuit Design.

2.1.2. Requirements and Specifications in the EEG Circuit: Case "1"

The given table outlines the exact requirements and specifications for this EEG circuit that include the following: Common Mode Rejection Ratio (CMRR) is greater than 120 dB; hence, high-performance proof in the minimization of noise and interference. Its bandwidth and frequency range are cut with a 3 dB passband from 0.3 to 40 Hz, tailor-made for EEG signals that include ensuring the major relevant frequencies of the brainwaves are effectively captured. This then becomes a demonstration of a low-cost effective circuit. The extracted signal level will be a big gain at low frequency and effectively extracted; this way, the quality of the extracted signal and the level of noise are highly diminished. Table 1 shows the requirement and technical description in case "1" low cost designed EEG.

Table 1. Comparison of the Key Technical Aspects of Medical-Grade & Research-Grade EEG Circuits.

Common Mode Rejection Ratio (CMRR)	Circuit Bandwidth	Signal Quality	Common Mode Rejection Ratio (CMRR)
>120 dB	0.3 to 40 Hz	▪ Gain: 25000 V/V ▪ Noise: absence of noise data ▪ Notch depth: 48 dB at 50Hz	▪ Notch only at 50Hz not 60Hz, ▪ Not input test data provided ▪ No test for strong muscle artifacts ▪ No ESD protection ▪ Not test for compliance with the safety standards for current

2.2. Battery-Powered, Low-Noise Amplifier Circuit Design of EEG Analog Front ends: Case ''2'

2.2.1. Description of Topology and Connectivity

This section presents the design of a battery-operated low-noise amplifier for an EEG application; it amplifies the signal of brainwave to some desired value. These designs are tailored toward signal amplification with only two active electrical parts and guaranteeing the high Common Mode Rejection Ratio (CMRR) at a level necessary to properly record the weak and small EEG amplitude signals. The system architecture for the active contains an inverting amplifier and other passive components, as shown in Figure 3. In the use of the device, a filter instrumentation amplifier was applied for low-passing the signals and frequency-dependent gain [48].

Preprints.org (www.preprints.org) | NOT PEER-REVIEWED | Posted: 3 June 2024 doi:10.20944/preprints202404.2023.v2

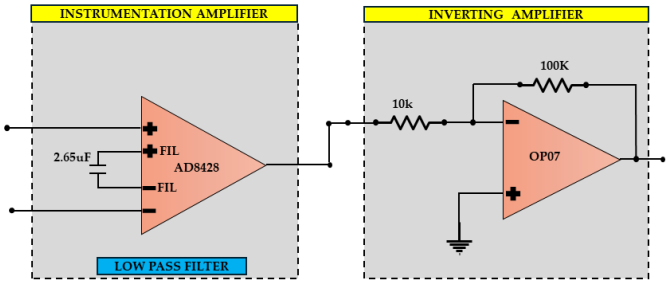

Figure 3. Battery-based EEG Signal Acquisition System (BB-ESAS).

2.2.2. Requirements and Specifications in EEG Circuit: Case "2"

The specific requirements and specifications of EEG Circuit set in [48] are supplemented with the technical characteristics of the AD8428 amplifier [49] for a thorough analysis. This circuit boasts a notable CMRR of 140 dB, effectively minimizing noise and interference by canceling out the common component of the two input signals. On the contrary, unlike the usual EEG frequency ranges, this circuit is specifically designed for a wide range of frequencies up to 3.5 MHz. Furthermore, the circuit is distinguished by its extremely low-cost design, achieved through the use of merely two components, thereby ensuring affordability. Moreover, the circuit excels in signal quality, with the Vpp noise from 0.1 Hz to 10 Hz being only 50 nV before amplification. Lastly, the circuit provides a variable gain up to 10580K V/V, a gain that is a strictly increasing function of frequency. The requirements and specifications for a battery-powered, low-noise EEG amplifier system are meticulously detailed in Table 2.

Table 2. Requirements and specifications in battery-powered, low-noise EEG amplifier system (Case "2").

Common Mode Rejection Ratio (CMRR)	Circuit Bandwidth	Signal Quality	Common Mode Rejection Ratio (CMRR)
140 dB	3.5 MHz	▪ Gain: variable 40.9K to 10580K V/V ▪ Noise: Vpp noise in 0.1 Hz to 10Hz is 50nV before amplification ▪ Notch depth: -	▪ No Notch at 50Hz or 60Hz, ▪ No test for strong muscle artifacts ▪ No ESD protection ▪ Not test for compliance with the safety standards for current

2.3. Double Notch Filter Circuit Design of EEG Analog Front ends: Case ''3''

2.3.1. Description of Topology and Connectivity

This subsection offers an elaborate examination of the structure of a high-performance EEG signal acquisition System. This device integrates a driven-right-leg feedback circuit, differential amplifier circuits, pre-amplification components, and multiple filters. The design incorporates both a pre-amplifier and a two-stage post-amplifier to efficiently amplify the signal. The circuit uses two low-pass filters and two 50Hz notch filters in order to reduce the occurrence of noise interference present in the raw EEG signal. In the pre-amplification stage, an instrumentation amplifier is used to ensure low levels of noise, minimal changes over time, a high input impedance, and a high CMRR. Moreover, the circuit incorporates a post-amplification stage that employs a high-precision chopper-

 doi:10.20944/preprints202404.2023.v2

stabilized operational amplifier. Aside from the post-amplification stage, additional filtration is implemented, namely two notch filters and a low-pass filter, to eradicate high-frequency noise resulting from differential interference [50]. A clarifying overview of this architecture is given in Figure 4 below.

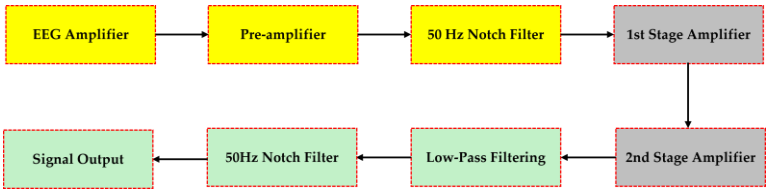

Figure 4. Double Notch Filter Circuit Design of EEG.

2.3.2. Requirements and Specifications in EEG Circuit: Case "3"

The specific requirements and specifications for this EEG circuit are well articulated. Although the CMRR is estimated at 110 dB, the circuit's bandwidth is adeptly configured from 0.5 to 33.86 Hz, which is within the mostly studied EEG signal frequency spectrum between 0.1 and 100 Hz. This illustrates the system's capability of effectively handling the bandwidth requirements that are essential for EEG signal processing. In terms of signal quality, the pre-amplification error is a minimal 0.74%, rising slightly to 1.75% post-amplification, indicating a high level of signal fidelity. Subsequently, the circuit is a budget-friendly choice due to its low cost. The requirements and specifications for a double notch filter analog front end EEG circuit is meticulously detailed in Table 3.

Table 3. Requirements and specifications in Double Notch Filter Circuit Design of EEG (Case "3").

Common Mode Rejection Ratio (CMRR)	Circuit Bandwidth	Signal Quality	Common Mode Rejection Ratio (CMRR)
Estimated at 110 dB	0.5 to 33.86 Hz	▪ Gain: 64000 V/V ▪ Noise: pre-amplification error: 0.74% ▪ Post-amplification error: 1.75% ▪ Notch depth: absence of depth data	▪ Notch only at 50Hz not 60Hz, ▪ Not input test data provided ▪ No test for strong muscle artifacts ▪ No ESD protection ▪ Not test for compliance with the safety standards for current

3. Materials and Methods: A Novel Proposed EEG Analog Front End Circuit System

With respect to the goal of this study, to our best knowledge in recent bibliography, there is a lack of EEG circuits that can combine concurrently, on the one hand, the monitoring of the theta, alpha, and beta brain wave frequency bands during usage time in which the user performs strong compound muscle movements (that is, the EEG usage protocol, or protocol named for simplicity in this study), and on the other hand, employing an EEG circuit that is mobile, low-cost, and with sufficient muscle artifact handling.

In this study, the design of a novel EEG Analog Front End Circuit System is proposed that can handle the problem; the aforementioned protocols containing compound muscle movements generate substantial muscular artifacts in the raw EEG data [24]. The electronic equipment requirements of this kind of protocol can be satisfied by a proposed System in this study, which is battery supplied in order to cover this mobility demand, uses simple and minimal sub-circuits to

 doi:10.20944/preprints202404.2023.v2

retain low cost (complex techniques such as chopping are avoided) and employs the necessary filters before and after the amplification stage to handle muscle artifacts sufficiently. The protocols for which the proposed system is designed could apply in neuro-feedback training, tele-controlling devices using Brain-Computer Interfaces (BCIs) in which the EEG user performs muscle compound movements [3,4]. Additionally, before implementing the simulation test, in this study, a realistic electronic model of the human brain and body is created that considers the factor of EMI from the external environment, in order to produce an accurate and mainly reproducible input signal to avoid the phenomenon of 'Garbage In, Garbage Out' (GIGO) during the evaluation of System. In the contemporary engineering terminology jargon, as presented in [51,52], GIGO is a concept that suggests that the quality of output in a system is determined by the quality of input. Incorrect input, such as incorrect data, can lead to incorrect output. GIGO is commonly used in mathematics and computer science but can also be applied to decision-making systems where precise data is crucial for accurate results. Figure 5 serves as a comprehensive overview of the circuit, providing a visual high-level reference that nonetheless includes all the elements and subcircuit of the EEG circuit.

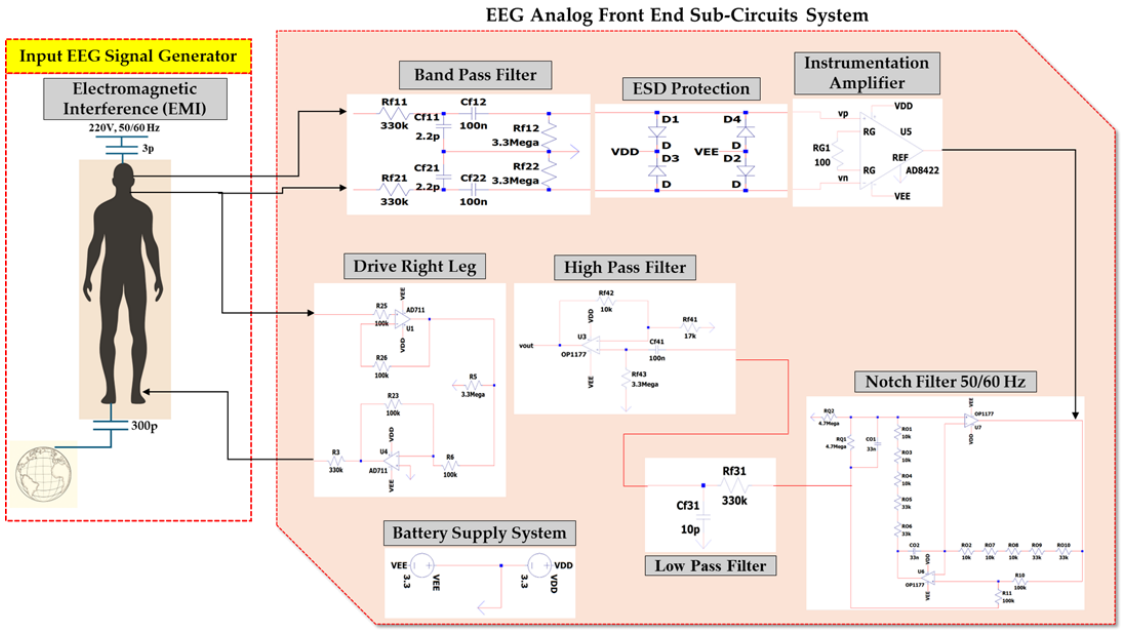

Figure 5. Visualization of Proposed EEG.

The aforementioned proposed EEG circuit design's requirements will be presented. Firstly, a Common-Mode Rejection Ratio (CMRR) greater than 90 dB is explained in [53]. Furthermore, the noise within the frequency range of 0.1 to 10 Hz is required to remain below approximately 500 nVpp root mean square noise [28]. The bandwidth of the input signal for this novel EEG is desired to denoise accurately, and it is from 0.5 Hz [53] to 3000 Hz in order to include a wide range of brain activity [54], with a specialized focus on the 4 Hz to 30 Hz frequency region. This special range of frequency is essential for monitoring the theta, alpha, and beta brain wave bands. Additionally, the circuit design demands a careful choice of a high input resistance, traversed by a maximum current of less than 10 μV, for human-user safety reasons. This complies with safety standards for medical or research environments. The selection of component values was made with consideration for future design iterations since the Printed Circuit Board (PCB) layouts need capacitors with a maximum value of 100 nF [46]. Prior to conventional designs, the proposed circuit specifically tackles notable issues; including inadequate filtering, limited bandwidth, and additional noise introduction prior to the amplification phase [47,48,50]. Our cost-effective approach aims to encourage research and commercial use while maintaining the high-quality signal integrity required in medical-grade applications. It does this by keeping the system simple with usage of the minimum number of components necessary to achieve the stated goal of the design. This goal is also achieved by avoiding more expensive component-wise circuits (in term of components and cost added versus accuracy

 doi:10.20944/preprints202404.2023.v2

gained) that implement techniques such as chopping. If accuracy is of importance and the designer of an application using this circuit wants to compromise cost over accuracy, using precision 0.1% resistors is advised, and in that spirit the theoretical calculations are provided with two decimal points digit point precisions. The requirements and specifications for the novel proposed circuit EEG design are detailed in Table 4.

Table 4. Requirements and specifications in the Novel Proposed EEG.

Common Mode Rejection Ratio (CMRR)	Circuit Bandwidth	Signal Quality	Common Mode Rejection Ratio (CMRR)
Greater than 90 dB	0.5 Hz to 20 kHz	▪ Noise within 0.1 to 10Hz: Below 500 nVpp root mean square noise ▪ Specialized Focus: 4 Hz to 30 Hz ▪ High Input Resistance: Max current < 10 μV	▪ Cost-effective ▪ Encourages research and home use. ▪ Maintains high-quality signal integrity. ▪ Simplifies system without complicated techniques such as chopping

In the next sections, the proposed EEG design will be presented as a series of sub-circuits for clarity and simplicity. With respect to which subcircuit is dedicated either to the creation of noise or to its reduction with respect to the EEG signal, the following stand true for the subcircuit of the subsection:

- 3.1: Simulates the EMI noise,
- 3.2: Simulates all types of muscle artifacts (noise stemming from either EMG, EOG, or ECG types of signals),
- 3.5: Provides a feedback loop between the circuit and the body that leads to the reduction of the overall noise and the possible sharp changes that may occur in the noise sources.,
- 3.6: Achieves an initial reduction of dc-offset and low-frequency and high-frequency noises,
- 3.7: Significantly reduces both EMI and artifacts that are contained in the common mode part of the input signal,
- 3.8: Eliminates the remaining EMI noise from the Main either at 50 Hz or 60 Hz depending on the region specific configuration of the circuit that is being used,
- 3.9: Eliminates the remaining high-frequency noises,
- 3.10: Eliminates the remaining dc-offset and the low-frequency noises.
- For detailed figures of each subcircuit (see Figures C.1-C.10), as well as exact calculations of the provided values and equations that govern the subcircuits in cases they are not provided in the subchapters (for space conservation reasons), please see Appendix C.

3.1. EEG Sub-Circuit Modeling the Electromagnetic Interference of Electric Grid with the Human Body

This sub-circuit is specifically engineered to replicate the voltage that an individual could encounter due to nearby electrical circuits linked to the power grid. In this model, resistive components symbolize the electrical loads in close proximity to the person, while capacitive components represent the medium of air through which electromagnetic waves propagate towards the human body. This design essentially depicts the network as a source of electromagnetic waves, with the human subject serving as the recipient. The primary purpose of this sub-circuit is to simulate, rather than reduce, electromagnetic interference, hence improving the accuracy of EEG signals by defining patterns of interference.

 doi:10.20944/preprints202404.2023.v2

3.2. EEG Sub-Circuit Modeling the Human Body Apart from the Brain and Earth

This sub-circuit models the relationship between the human body and the Earth, including muscle movements and heart activity, which generate electrical interference in the EEG signal. Resistances are crucial for accurately replicating physiological electrical circuits, both between the head and body, and between the body, ground, and reference electrode. Physiological sounds, namely complicated muscle movement artifacts, are identified as having a frequency range of 1-200 Hz and an amplitude range of 0.1–100 mV, based on empirical data and study results [24].

More precisely, the sub-circuit converts muscle noises into voltage sources that occur at various locations throughout the EEG recording process. This is performed in order to compute the mean intensity of the alpha, beta, and theta signals. It mimics biological tissue by using a series of voltage sources and resistors to reduce electrical thermal noise, a phenomenon that is typical in electronic components but absent in actual tissues. According to the empirical results of the experiments related to electrode's voltage measurement during protocols with compound muscle movement, performed in the ''Biomedical Optics & Applied Biophysics Laboratory'' of the School of Electrical and Computer Engineering of the National Technical University of Athens, the voltage sources are configured within the range of 1-80 Hz and 1-50 mV. The aim of these experiments was to capture peak-to-peak (Vpp) raw EEG signals by employing wet electrodes during the performance of intricate muscle movements, such as jumping and walking.

Furthermore, to simulate the body's grounding phenomenon, the modeling incorporates resistances across various anatomical regions and 300 pC capacitors. In particular, these resistances are modeled as noiseless because, in contrast with their electronic counterparts, those in between tissues do not yield thermal noise in the context of our model. The result is a closed-loop system between the Earth and the EMC model of the human body.

3.3. EEG Sub-Circuit Modeling the Brain and the Electrode

The objective of this circuit element is to emulate the voltage signals generated by the human brain. The simulation incorporates voltage sources to represent brain signals across the alpha, beta, delta, and theta wave bands, with amplitudes precisely measured in μV. This method enables the precise depiction of the brain's electrical activity, including a spontaneous event-related potential (ERP) with a high frequency of 2930 Hz. The investigation of such a high-frequency ERP is often conducted using intracranial electrodes, highlighting the advanced nature of our model in accurately representing a wide range of neuronal activity [54].

The deliberate incorporation of test sources containing an extensive range of signals is a strategic decision made to verify the accuracy of our EEG circuit in extracting the specific bands of interest for the intended protocol. When quantifying the alpha, theta, and beta frequencies during complex muscle movements, it is vital to account for this variable. It is possible to integrate wet electrodes with impedances between 1 and 50 kΩ into the circuit, modeled as a simple resistance. However, wet electrodes exhibiting impedances greater than 50 kΩ are customarily excluded from the system as a result of the compromised signal quality. Furthermore, this EEG circuit can be utilized with dry electrodes, which have impedances between 700 kΩ and 1400 MΩ. It must be noted that the impedance values of the electrodes, either wet or dry, are expected not to be equal.

3.4. EEG Sub-Circuit Modeling the Battery Supply of the System

The EEG sub-circuit is designed to model the power supply mechanism of the EEG circuit. This sub-circuit utilizes two 3.3V rechargeable batteries, similar to other battery systems found in contemporary mobile devices. encompasses this duality. Its battery supply system employs a special grounding symbol for representing the circuit's ground, depicted as an inverted lambda "Λ" Greek alphabetical symbol. This symbol is connected to a RC network, with R = 0.01 EΩ and C= 1zF in parallel. This network creates EEG circuit's ground by being connected to Earth grounding on one end and the intersection between the two batteries and the circuit's ground on the other end. The design incorporates a closed triangle to represent the Earth's ground and an open triangle to represent

 doi:10.20944/preprints202404.2023.v2

the circuit's ground. This configuration is a mandatory design requirement, because of the selected simulation software program's limitations in supporting two Earth symbols (a symbol with precisely 0V AC and 0V DC voltage source references). The circuit's ground exhibits a DC voltage of 0V and an AC voltage of 200pV; thus, it is safely considered for the rest of this study to be a 0V reference while being independent from the Earth's ground.

3.5. EEG Sub-Circuit Modeling the Driven Right Leg (DRL) Circuit

The utility of the DRL circuit is the creation of a feedback loop between the reference electrode and the body. This arrangement incorporates meticulously chosen resistors to protect both the electronics and the user. The circuit utilizes signal inversion and redirects it towards the body in order to ensure that the current remains below the safety threshold of 10μA, as required by IEC-601-1 safety rules [31,32]. This sub-circuit is powered by a battery with a maximum voltage of 3.3V. A 300 kΩ resistor is used to regulate the maximum current to 10 μA, although typical operational currents fall within the range of several hundred nA. This configuration showcases our commitment to safety by ensuring that the circuit operates smoothly within predefined limits under normal conditions.

Additionally, a 3.3MΩ resistor serves as a crucial pathway for the movement of leakage current towards the ground in the event of a malfunction. The primary function of this high-resistance component is to operate with a very low level of current, often within the nA range. This guarantees that the EEG signal remains undistorted when it is reintroduced into the body via the dual buffer amplifiers. A 100kΩ resistor is used to optimize the circuit's efficiency and minimize power consumption. The choice was made to retain the feedback current usage at around 0.5 μA. This strategy not only maintains the longevity of the battery but also ensures minimal energy consumption from the system. The intentional design strategy is opting for a larger resistor rather than a smaller one to attain an optimal equilibrium between power efficiency and operational effectiveness.

3.6. EEG Sub-Circuit Modeling the First Band-Pass Filter

This sub-circuit is precisely designed to achieve two specific goals: (i) safeguarding the user of the novel EEG circuit, and (ii) simultaneously constructing a traditional RC band-pass filter. The positioning of the high-pass filter at the beginning of the band-pass filter sub-circuit accounts for the fluctuating resistance characteristic of the electrode contact. The high-pass filter has an input resistance of 330 KΩ. The indicated quantity is the minimum requirement to adhere to safety regulations, which restrict the amount of input to the body to a maximum of 10μA, as specified by IEC-601-1 safety rules.

A 2.2 pF capacitor was used to ensure that, despite the dry electrode's greatest input resistance of 1.4 MΩ in combination with the 330 KΩ resistor, the filter effectively includes the highest frequency of interest, 20 kHz, inside the pass band's 0 dB gain range. The exact configuration of electrode resistances yields cutoff frequencies ranging from 41.81 kHz (with an input resistance of 1.73 MΩ) to 218.56 kHz (with an input resistance of 331 KΩ).

Furthermore, a first high-pass filter is used at around 0.4822 Hz to eliminate any variations in DC offset and somewhat reduce muscle interference, while having negligible impact on the signal prior to amplification. While a cutoff frequency of 0.05 Hz or lower would be ideal for preventing signal distortion, implementing such a low frequency would necessitate the use of excessively large capacitors. This is especially true in scenarios where there is substantial muscle noise, such as during physical exertion or when experiencing the revival of embodied psychological trauma. Therefore, making slight adjustments to the EEG signals in the delta wave region is an intentional choice that aims to find a compromise between the accuracy of signal capture and the practical limitations imposed by significant muscle interference.

3.7. EEG Sub-Circuit Modeling the ESD Protection and the Instrumentation Amplifier

This After the output of the band-pass filter, the design integrates electrostatic discharge (ESD) protection utilizing the circuit proposed in [55]. This sub-circuit guarantees the safety of the EEG

 doi:10.20944/preprints202404.2023.v2

circuit and of its user, by creating a path to the positive and negative supplies for transient electrical currents that may arise from contact between objects with disparate electrical charges, known as the ESD protection circuit.

Consequently, the signal is passed to the instrumentation amplifier, which has as input both the channel one electrode and the reference electrode. The amplifier has a gain of 199 V/V and reaches 99.9999% of its maximum value in approximately 15 μsec of settling time. The AD8422 is chosen as an instrumentation amplifier because of its CMR performance. It has a specific CMRR of 110 dB, much over the minimum requirement of 90 dB [29]. The resistance of the gain resistor RG is set to 100 Ω, ensuring a theoretical gain of G = 199 [56].

3.8. EEG Sub-Circuit Modeling the Fliedge Notch Filter 50Hz or 60Hz

Active notch filters are used to attenuate significant aberrations occurring at 50 and 60 Hz in EEG data. They have shown challenges in terms of adjusting the center frequency, maintaining stability, and achieving repeatability. The maximum goal that the designer could achieve, is a noise level reduction of approximately 40 to 50 dB when simulating the circuits by theoretical calculations. Consequently, this design prioritizes center frequency and Q above notch depth. The Q value of a certain notch filter corresponds to the frequency at which the filter's response is attenuated by -3 dB, not at the point 3 dB above the notch depth.

This is a dual operational amplifier filter that utilizes just four high-precision components: (i) two resistors (Ro) and (ii) two capacitors (CO). These components are responsible for setting the damping factor and center frequency of the filter. RO resistance is shown as an assemblage of resistances that possess a high level of accuracy. Circuits that are used in a 50Hz grid make use of resistors RO6 and RO10 with a resistance of 33 kΩ (see Figure 6 or Figure C.8 in Appendix C for more details). It is necessary to place an extra 33kΩ resistance in parallel with RO6 and one with RO10 respectively, in order to utilize the EEG in a 60Hz grid environment.

The Q factor of the filter may be modified separately from the center frequency by using two resistors of equal value that are not sensitive to changes. The center frequency of the filter may be modified within a defined range without significantly reducing the depth of the notch. A greater Q factor results in a smaller stopband, but this comes at the cost of a reduced depth of notch at the desired center frequency [57]. In the case of the 50Hz grid the center frequency and Quality factor are:

$$f_o \approx 50.24 \text{ Hz and } Q \approx 24.48$$

In contrast, we employ the 33 kΩ resistance parallel to RO6 and RO10 (see Figure 6 or Figure C.8 in the Appendix C) for the 60Hz grid, center frequency and Quality factor are as follows:

$$fo \approx 60.67 \text{ Hz and } Q \approx 29.56$$

respectively. The proposed notch should theoretically achieve a notch depth of 50 dB at the center frequency calculated above.

3.9. EEG Sub-Circuit Modeling the Second Low Pass Filter

This sub-circuit is a simple RC low pass filer, with 3 dB cut-off frequency:

$$f_c \approx 48.23\ KHz$$

This cut-off frequency is in accordance with our design requirements because the input raw EEG signals of interest have maximum frequency of 20 kHz. Indeed, the 20 kHz frequency resides well within 0 dB gain part of the passband of our high-pass filter with upper frequency of 48.2 kHz. The settling time to a steady state value from 0% to 99.99% is achieved after 30.39 ms with this design.

3.10. EEG Sub-Circuit Modeling the Second High Pass Filter before the Analog to Digital Conversion

In this section, a Butterworth filter is implemented in order to exploit its characteristic that it does not allow ripples in the passband while also helping us create a further gain of approximately

 doi:10.20944/preprints202404.2023.v2

1.5 V/V in the wave bands of interest [57]. The two important parameters that characterize the Butterworth filter are AF gain and fl cutoff -3 dB frequency, which in the proposed circuit have the values:

$$A_F \approx 1.59 \; and \; f_l \approx \; 0.48 \; Hz$$

If ''f ''is the frequency of the input signal the magnitude of the voltage gain is:

$$\left|\frac{V_{out}}{V_{rchpf}}\right| \approx \frac{3.29 * f}{\sqrt{\left(1 + \left(\frac{f}{0.48}\right)^2\right)}}$$

3.11. The Overall Novel EEG-B3V3S7C1 Circuit Design

The overall EEG Circuit Design has a bandwidth of approximately 0.5 Hz to 10 kHz, an overall gain of 300 V/V in the passband, and a theoretical CMRR of 110 dB. In Figure 6 (Figure 6 is presented for an high level visualization of the topology, independent pictures of the subcircuit are in Appendix C), the overall EEG Circuit Design named EEG-B3V3S7C1 (named inspired by the characteristic batteries of 3.3V, 7 sub-circuits, and 1 channel). The noise of our design before the first amplification will be estimated as the total Vpp noise in the equivalent noise bandwidth range of 0.1Hz to 10Hz, and was a value of ent≈779.32 nV.

The design of this EEG circuit did not include an anti-aliasing filter due to its focus on the analog front-end (AFE) and neglecting the digitization process. An anti-aliasing filter reduces frequencies above the half of the sampling frequency towards zero. The design of an Anti-Aliasing filter must consider the sampling frequency of the ADC, and the low pass filter of the proposed circuit can be used as an antialiasing filter, but only in the special case the ADC's sampling frequency is double to or greater than the cutoff frequency. So,

Preprints.org (www.preprints.org) | NOT PEER-REVIEWED | Posted: 3 June 2024 doi:10.20944/preprints202404.2023.v2

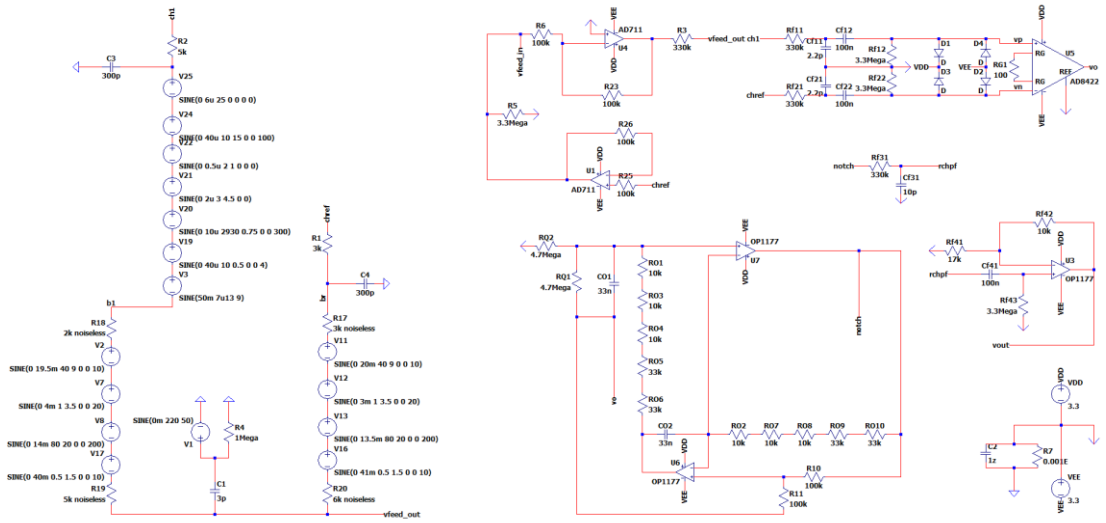

Figure 6. The Overall Novel EEG-B3V3S7C1 Circuit Design.

4. Simulation and Results: Comprehensive Analysis

The initial goal of the simulation is to quantify the difference between theoretical value predictions for the different subcircuits and real-world simulated implementation values of the proposed novel EEG-B3V3S7C1 circuit design. In particular, this simulation of the circuit's electronic behavior can assess the design's efficiency because it provides accurate voltage and current waveform representations, verifying that the authors' pre-defined requirements for the circuit are met in a satisfactory percentage. Moreover, another goal is to visualize the human body and environment model signal generator's output, assessing its realisticness and its alignment with laboratory experiment results. Furthermore, it is given emphasis on examining the EEG output in the following ways:

- Time domain to make a qualitative commenting in regard to CMRR, power consumption, gain, and noise level before the first amplification.
- Fourier frequency spectrum to validate if the information in the alpha, beta and theta wave bands is preserved.
- Fourier frequency spectrum and time domain to validate that the compound muscle movement artifacts are sufficiently suppressed.

The simulation is carried out both in a 50Hz and 60Hz power grid environment because these frequencies cover the most common EEG signal measurement cases that are not performed in a shielded environment of electromagnetic interference from the power grid [58]. Subsequently, a comprehensive comparison is conducted between the proposed novel EEG-B3V3S7C1 circuit design's simulated results and those of the cases ⅼ"1", ⅼ"2", ⅼ"3" that were presented previously in this work.

This section is divided into two segments: (A) the simulation of the circuit in the time and Fourier analysis frequency domain, and (B) the comparison of the proposed Circuit (EEG-B3V3S7C1) with the cases ⅼ"1", ⅼ"2", ⅼ"3" as follows.

4.1. Simulation of Novel EEG-B3V3S7C1 Circuit Design

As it is known by the circuit design section, our circuit includes the reference electrode for calculating the voltage reference of the collected raw EEG signal as well as the Channel 1 electrode for collecting the raw EEG signal. According to their functionality, the first is placed behind the ear, and the other is placed on the Fp1 position (10-20 positioning system) [25]. The main purpose of this test is to simulate the characteristics of the circuit that were deemed important when deciding the requirements of the circuit presented in this study, namely CMRR, bandwidth in the 0.5Hz to 3kHz

 doi:10.20944/preprints202404.2023.v2

region, and in particular in the 4Hz to 30Hz alpha, beta, and theta wavebands range. Another crucial element that must be examined in this simulation is the notch depth of the notch filter when it is functioning at approximately either 50Hz or 60Hz frequencies. Finally, a visual representation of both time and frequency responses will be presented further down to showcase the effectiveness of the circuit. In particular, it examines the circuit's ability to denoise the artifacts of the raw EEG signal acquisition process in the presence of strong compound muscle movements while preserving the signal integrity of the alpha, beta, and theta wavebands.

4.1.1. Simulation in a 50 Hz Electrical Grid Environment

In this part, the simulation in a 50 Hz environment is performed. The CMRR of the circuit was assessed by short-circuiting the two input channels with a voltage source of 0V DC offset and 1V AC amplitude across all frequencies. While performing AC analysis, the CMRR yielded a frequency response function dependent on the frequency variable. In the band of interest of alpha, beta and theta waves, CMRR was approximately 97 dB. In frequencies greater than 166 Hz, CMRR dropped below 90 dB and at 3 kHz reached 66 dB. Meanwhile, in the area below 1 Hz, CMRR reached levels up to 163 dB at 10 mHz. The simulated notch depth was measured at 48.5 dB, which is a really satisfactory result based on [56], which defines realistic expectations for maximum realizable notch depth between 40 dB and 50 dB. Apart from the above evaluations, noise analysis was performed on the circuit. The result of 1.4887μVpp noise in 0.1 Hz to 10Hz before amplification was identified in a 50Hz environment. The total power consumption was measured at approximately 20.5 mWatt. The simulation at 50 Hz produces results in the time domain by performing transient analysis (see Figures 7 and 8).

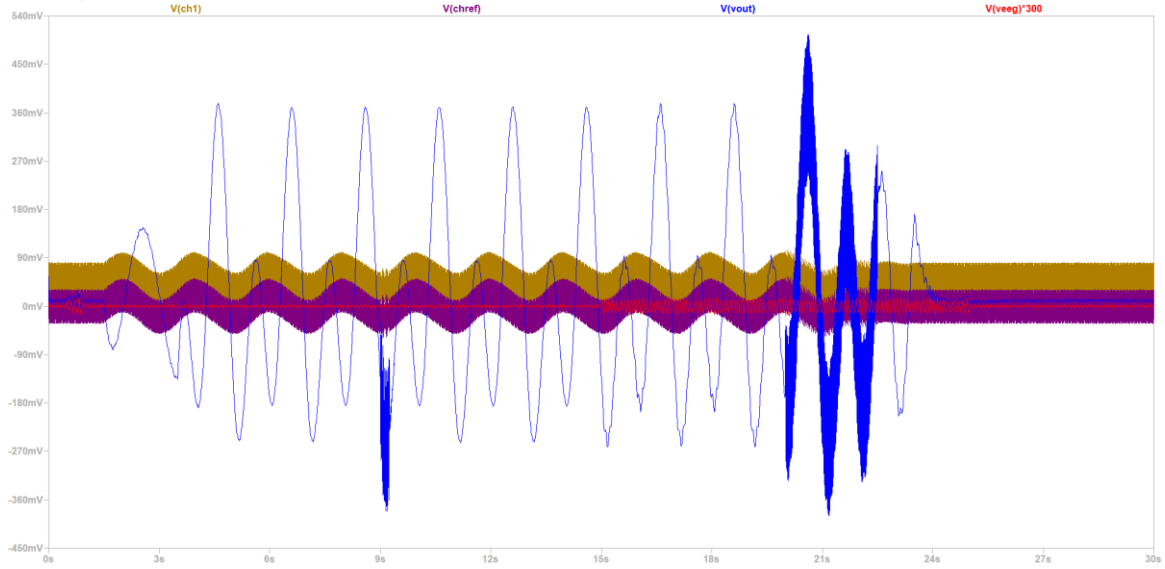

Figure 7. Time response of the simulation. Waveforms: Raw EEG Channel 1 signal – Purple, Raw EEG reference channel signal – Gold, Ground truth EEG signal - Red, Output of the EEG circuit – Blue.

Consequently, with the use of FFT algorithm, the Fourier transform results in the Fourier plane are also generated (see Figures 9–13).

- *Simulation at a 50 Hz Electrical Grid Environment in the Time Domain*

Initially, the simulation (at 50 Hz) focused on demonstrating that our design was able to generate realistic electrode signals, similar to the ones measured in the laboratory experiments during the performance of compound muscle movements. As it is depicted in Figure 7, the gold waveform is the voltage measured at the reference electrode (V_{chref}). The purple waveform is the voltage measured at the Channel 1 electrode (V_{ch1}). The red waveform depicts the EEG ground truth signal contained in Channel 1 (V_{eeg}), magnified 300 times for clarity. The blue waveform is the output of the EEG-B3V3S7C1 circuit design (V_{out}).

 doi:10.20944/preprints202404.2023.v2

By observing Figure 7 it can be assessed that the output signal in blue clearly resembles the ground truth signal in red, apart from a 14.5 mV DC offset and muscle noise artifacts. The muscle artifacts remaining in the output signal produce low frequency sine-like waves like the one shown in Figure 7, which nonetheless still carry all the important information of the EEG signal (it resembles the phenomenon of signal modulation). Indeed, the strong muscle compound movement artifacts are severely suppressed and don't influence the measurement capability of the proposed circuit, as it will become clear on the following subsection, where it becomes apparent that the remaining noise artifacts do not forbit the detection of alpha and beta wave peaks in the Fourier Plane. By looking closer at Figure 8, several facts about the morphology of the EEG signal can be observed. The red signal represents the component of the brain signal that is collected by the electrodes of the EEG circuit. In order to visualize it in the image the raw EEG signal is magnified 300 times, in order to be on the same order of magnitude with the actual raw signal that is collected by the electrodes. It contains the slower but bigger in amplitude alpha wave component from approximately 0.3 s to 0.8, as well as some faster lower amplitude beta and gamma wave components. Noteworthy is the segment in the region of around 0.8 s, where a higher frequency ERP phenomenon of around 3 kHz is depicted.

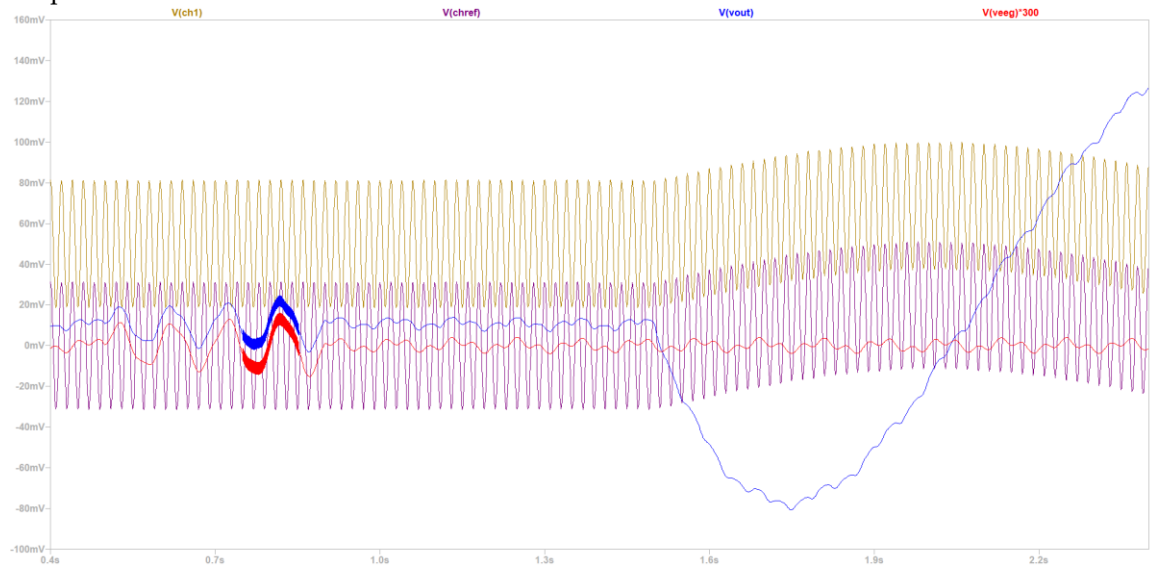

Figure 8. Time response of the simulation. Waveforms: Raw EEG Channel 1 signal – Purple, Raw EEG reference channel signal – Gold, Ground truth EEG signal - Red, Output of the EEG circuit – Blue. This picture presents the same experiment as Figure 7 but time course of the experiment is limited from 0.4 to 3s.

The gold signal is the one from the electrode that carries the brain red signal, while the purple signal is the one of the reference electrode. The morphology of those waveforms validates the proper functionality of the proposed signal generator circuitry, because it accurately depicts EMI noise and muscle artifacts that have contaminated the raw EEG brain signal. More precisely, EMI is the higher frequency component of the purple and gold waveforms at around 60 mVpp and the slower but rather higher amplitude component of the waveforms that carries on top of it the EMI noise is the one that relates to muscle movement artifacts (i.e. EMG, EKG, EOG) that the electrodes collect.

The blue line is the output of the EEG circuit. It takes the raw EEG signal and magnifies it by 300 V/V, as it was theoretically expected validating the design. Moreover, it achieves an extreme reduction of both the EMI noise and of the muscle artifacts. Instead of being magnified 300 times, the first is hardly inspectable in the output signal and the second is magnified at around only 2 times. This ensures that this novel design successfully suppresses EMI and muscle noise artifacts, ensuring satisfactory EEG signal acquisition.

- *Simulation at 50 Hz Electrical Grid Environment at the Fourier's Spectrum*

 doi:10.20944/preprints202404.2023.v2

Subsequently, FFT was performed in the time domain produced by the transient analysis of the simulation (at 50 Hz) to generate the waveforms in the Fourier plane (in a range from 4 Hz to 30 Hz). The frequency response of waveforms in the Fourier plane gives valuable insights into the simulated functionality and performance of the circuit. As it is depicted in Figure 9, the green waveform is the voltage measured at the reference electrode (V_{chref}). The blue waveform is the voltage measured at the Channel 1 electrode (V_{ch1}). The pink waveform depicts the EEG ground truth signal contained in Channel 1 (V_{eeg}). The cyan waveform is the output of the EEG-B3V3S7C1 circuit design (V_{out}). Lastly, the red waveform is the voltage at the output of the instrumentation amplifier (V_{vo}). This waveform is the Fourier plane of the experiment when the Fourier Transform is performed from 0 sec to 3 sec and the plane is limited from 4 Hz to 30 Hz in linear x-axis scale, in order to more closely inspect the integrity of the signal in the wavebands of interest namely alpha, beta and theta.

Figure 9. Frequency response of the simulation (in a range from 4 Hz to 30 Hz). Waveforms: Raw EEG channel 1 signal - Blue, Raw EEG reference channel signal - Green, Ground truth EEG signal - Pink, Output of the EEG circuit - Cyan, Output of the instrumentation amplifier - Red. This picture presents the same experiment as Figure 7.

First and foremost, by observing Figure 9, it can be clearly assessed that the ground truth EEG signal integrity is preserved. This is apparent because in the picture the original raw brain signal is magnified 300 V/V and matches exactly the cyan waveform of the output in the desired peaks, in the case at 9 Hz, 10 Hz and 25 Hz, where beta and alpha wave consecration of power exists. Simultaneously, the noise artifacts do not affect the appearance of the brain signal peaks, but affect in a non-detrimental way for BCI of neurofeedback applications the rest of the EEG frequencies in the wavebands of interest. Thus, it is apparent from the graph that the circuit output gives the magnitude and, after some processing, the energy content for the alpha, beta and theta wave bands in thirty-second intervals, while the user of the EEG circuit participates in protocols with strong compound muscle movements. In Figure 10, where the same 30 s experiment is presented, in which the Fourier transformed is performed for only the first 3 s, the same observations as above still hold. So, it can safely be assumed that the circuit performs as intended both at single digit second intervals as well as tens of seconds intervals, satisfying the requirement for a wide range of neurofeedback and BCI applications. As far as EMI is concerned by inspecting the blue and green waveform that represents the signals collected in the electrodes, in Figure 10 the Main noise is at around -27 db (in this case of a 50 Hz grid), while in the output it is suppressed at approximately -74 db, validating the theoretical predictions about the depth of the notch filter. Moreover, it is apparent that the relative amplitude of the weakened EMI signal component in the output is in the order of magnitude of an extremely weak gamma signal, so the majority of gamma signals in the 50 Hz region could be collected by the proposed novel circuit of this study. This observation of course is also true for the conditions of Figure 9.

Preprints.org (www.preprints.org) | NOT PEER-REVIEWED | Posted: 3 June 2024 doi:10.20944/preprints202404.2023.v2

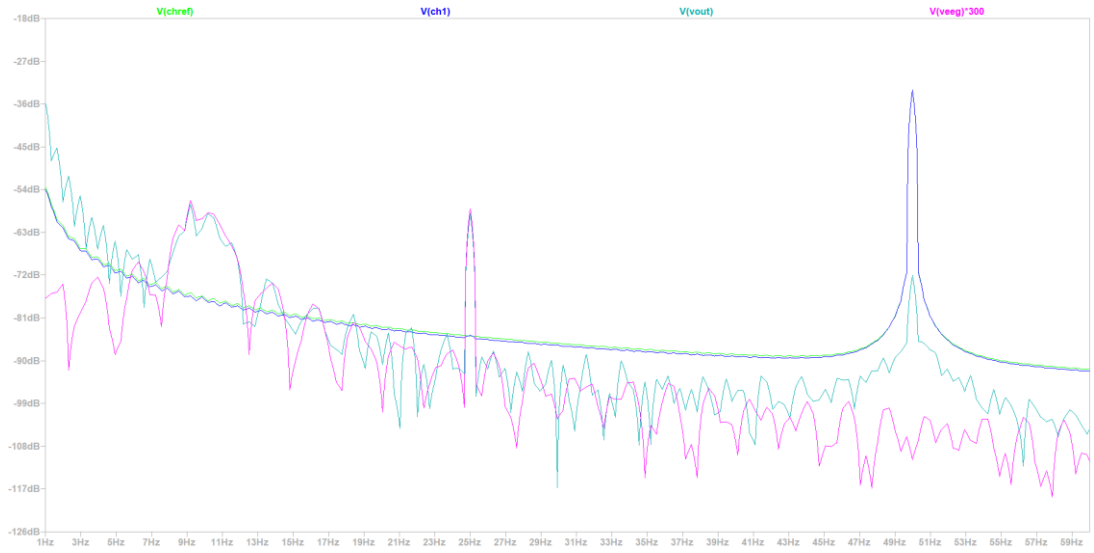

Figure 10. Frequency response of the simulation (in a range from 4 Hz to 30 Hz). Waveforms: Raw EEG channel 1 signal - Blue, Raw EEG reference channel signal - Green, Ground truth EEG signal - Pink, Output of the EEG circuit - Cyan, Output of the instrumentation amplifier - Red. This picture presents the same experiment segment limited from 0.4 to 3s as Figure 8.

As for Figure 11, it has the same ranges in time scale and Fourier transform as Figure 10, but it is consecrated in the 3 kHz region. As previously described, there is the region where the frequency component is expected to be of the ERP signal that takes place in the first second of this exemplary protocol presented earlier in the results. Indeed, a closer observation reveals that almost none of the original pink raw EEG signal is detectable in the green and blue waveforms that are collected from the electrodes, and the region is significantly contaminated by high frequency noise artifacts. Notably, the circuit can recreate the frequency information and especially the peak in the Fourier Plane of the ERP signal, validating that both filtering and amplification of our proposed circuit work as intended.

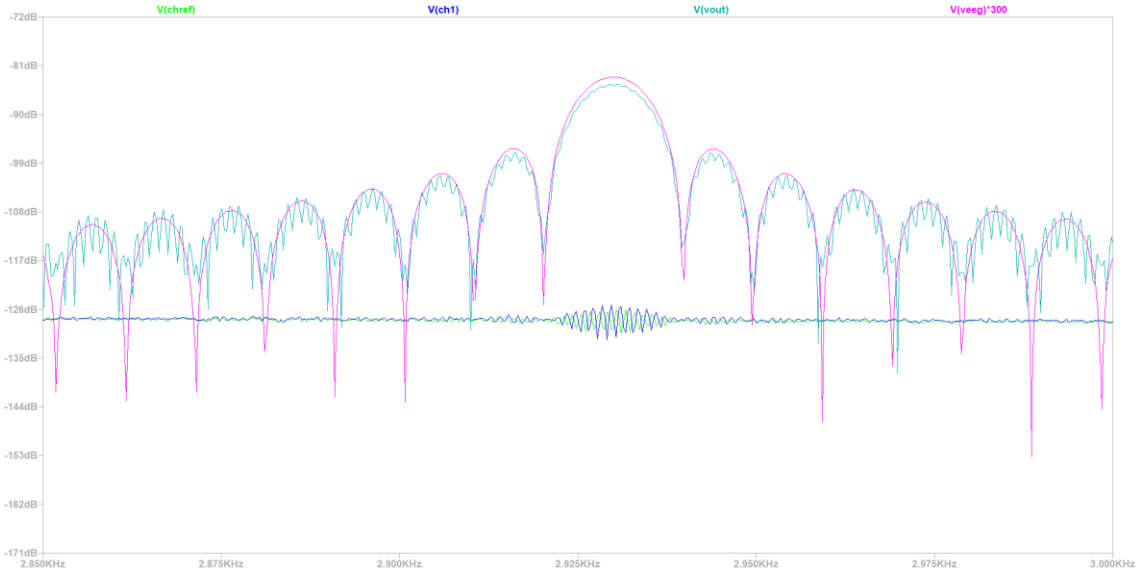

Figure 11. Frequency response of the simulation (in a range from 2.85 kHz to 3 kHz). Waveforms: Raw EEG channel 1 signal - Blue, Raw EEG reference channel signal - Green, Ground truth EEG signal - Pink, Output of the EEG circuit - Cyan, Output of the instrumentation amplifier - Red. This picture presents the same experiment segment limited from 0.4 to 3 s as Figure 8.

 doi:10.20944/preprints202404.2023.v2

Figure 12 represents the spectrum of the Fourier of the same constraints in time that were outlined for Figures 8, 10 and 11. The green waveform is the voltage measured at the reference electrode (V_{chref}). The blue waveform is the voltage measured at the Channel 1 electrode (V_{ch1}). The pink waveform depicts the EEG ground truth signal contained in Channel 1 (V_{eeg}), magnified 300 times. The cyan waveform is the output of the EEG-B3V3S7C1 circuit design (V_{out}). The red waveform is the voltage at the output of the instrumentation amplifier (V_{vo}), magnified 1.5 times.

First and foremost, it is evident that the real gain of the high pass filter subcircuit following the instrumentation amplifier is approximately 1.5 V/V, which is a value very close to the theoretical prediction of 1.59 V/V, verifying the accuracy of our design. Additionally, the real gain of the overall circuit is approximately 300 V/V, very close to the theoretical prediction of 316.01 V/V (199*1.59 = 316.01), which aligns with the predefined design requirements of the proposed circuit design. As it is depicted in Figure 12, the ERP signal is well preserved and denoised in the output of the signal. Notably, it can be clearly assessed that both the EMI and the muscle noise are significantly reduced. The blue and green peaks that exist in the vicinity of 50 Hz are reduced to a magnitude that is in the order of magnitude or less than the brain signal. Muscle artifacts are negligibly affecting the output signal.

Afterwards, in the same product of FFT analysis from the previous sub-section, the Fourier spectrum was examined in a bigger range from 10 mHz to 3 kHz, studying the same waveforms in the entire circuit's output bandwidth, as specified in the requirements of the proposed circuit design (0.5 kHz to 3 kHz). The aim of this approach was to confirm that in any range from 0.5 kHz to 3 kHz, including the frequency range of special interest from 4 Hz to 30 Hz, the ground truth EEG signal integrity is maintained, and at the same time, the noise artifacts do not influence the distinctiveness of the brain signal peaks. In Figure 13, again it is evident that the peaks in the alpha, beta and theta wave bands and of the ERP signal of the amplifiers output, the output of the total circuit and of the original brain waves, are all aligned. The muscle noise is suppressed and can has a significant presence in the output only in the frequency ranges below 1 Hz, affecting only the delta waveband, and mostly in the region of this band that is more rarely studied.

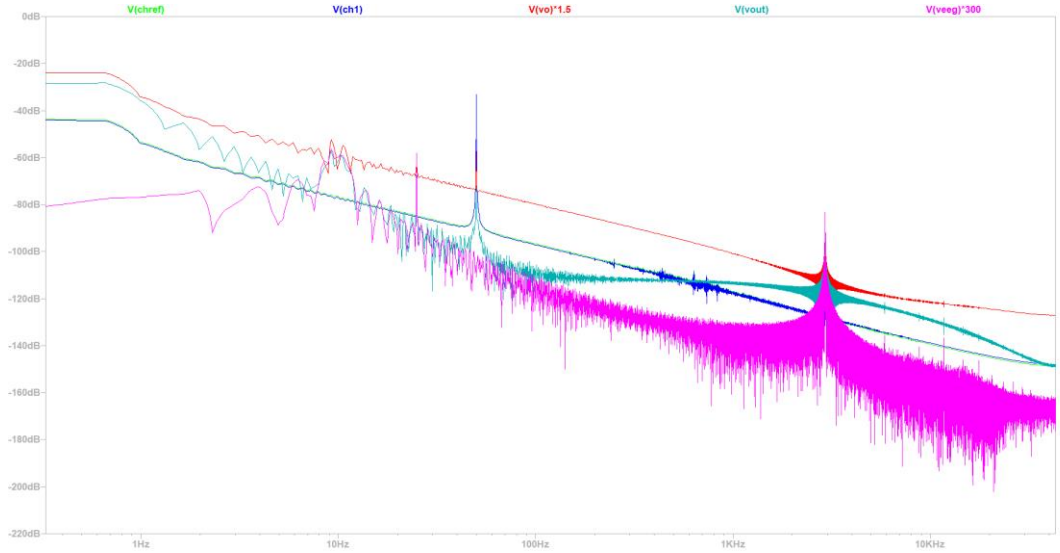

Figure 12. Frequency response of the simulation (in a range from 10mHz to 3kHz). Waveforms: Raw EEG channel 1 signal - Blue, Raw EEG reference channel signal – Green, Ground truth EEG signal - Pink, Output of the EEG circuit - Cyan, Output of the instrumentation amplifier – Red. This picture presents the same experiment segment limited from 0.4 to 3s as Figure 8.

Preprints.org (www.preprints.org) | NOT PEER-REVIEWED | Posted: 3 June 2024 doi:10.20944/preprints202404.2023.v2

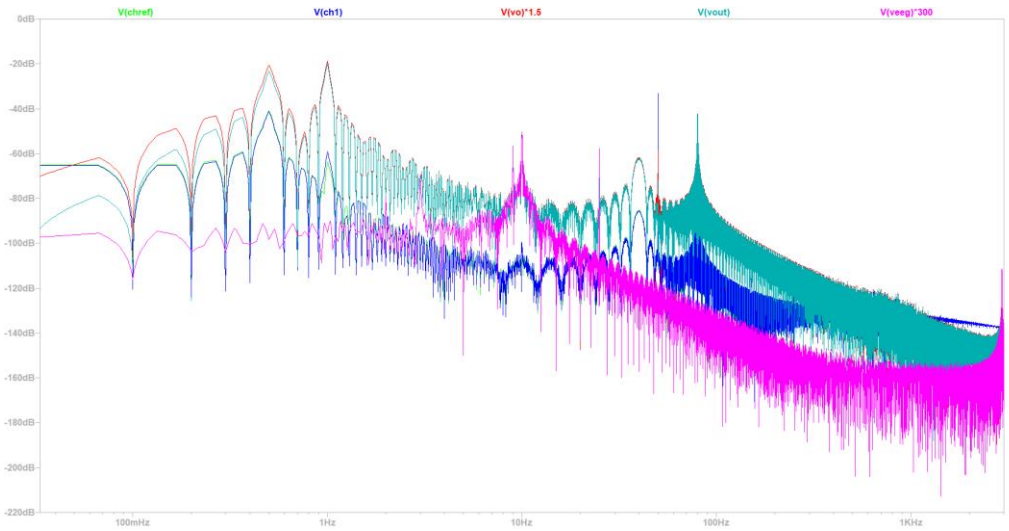

Figure 13. Frequency response of the simulation (in a range from 10mHz to 3kHz). Waveforms: Raw EEG channel 1 signal - Blue, Raw EEG reference channel signal – Green, Ground truth EEG signal - Pink, Output of the EEG circuit - Cyan, Output of the instrumentation amplifier – Red.

4.1.2. Simulation in an Environment with an Electrical Grid with Frequency 60 Hz

The same simulation, as previously analytically described, was performed in a 60 Hz power grid environment. It is obvious that this simulation produced the corresponding time and frequency domain simulation graphs, which are not presented in this subsection, for reasons of space conservation. The overall results were deemed satisfactory. Specifically, the CMRR of the circuit was assessed by short-circuiting the two input channels with a voltage source of 0V DC offset and 1V AC amplitude across all frequencies. While performing AC analysis, the CMRR yielded a frequency response function dependent on the frequency variable. In the band of interest of alpha, beta and theta waves, CMRR was approximately 98 dB, which is a slightly better performance than in the 50 Hz case. In frequencies greater than 110 Hz, CMRR dropped below 90 dB and at 3 kHz reached 62 dB. Meanwhile, in the area below 1 Hz, CMRR reached levels up to 163.5 dB at 10 mHz, similar to the 50 Hz case. The simulated notch depth was measured at 39.5 dB, which is acceptable, based on [56], which defines realistic expectations for maximum realizable notch depth between 40 dB and 50 dB, but is not as good as in the 50 Hz scenario.

Noise analysis was performed on the circuit for the 60 Hz configuration. The result of 1.4887μVpp noise in 0.1 Hz to 10Hz before amplification was identified in a 50Hz environment. The total power consumption was measured at approximately 20.5 mWatt.

4.2. Comparative Analysis of the Simulated EEG-B3VS7C2 with the Cases 1, 2, 3

As depicted in Table 5, with regards to CMRR, the proposed circuit is in alignment with the specification that demands values greater than 90 in the area of interest of the alpha, beta and theta wavebands. The maximum CMRR in the passband of our output signal is 97 dB and 98 dB at 50 Hz and 60 Hz, respectively.

It must be stated that this proposed circuit has been designed in order to focus on meeting the requirements of protocols with compound muscle movement. The satisfaction of these requirements necessitates filtering of the noise artifacts before the first amplification in order to protect the amplifier from reaching a state of saturation by amplifying undesired muscle artifacts that are present in the raw EEG signal. The introduction of filters at the initial stage limits the possibility of increasing the CMRR in any EEG analog front end. The only technical obligation of the proposed circuit with respect to CMRR is to be higher than 90 dB in the frequencies of interest, so any values higher than this lower limit can be considered acceptable. Thus, even though our CMRR is lower than the ones of the other Cases ‘‘1’’, ‘‘2’’ and ‘‘3’’ (110 dB up to 140 dB), this was a deliberate trade-off. The high CMRR of Cases ‘‘1’’, ‘‘2’’ and ‘‘3’’ is practically useless for the case of muscle movement artifact

 doi:10.20944/preprints202404.2023.v2

removal, because the aforementioned circuit has neither been tested for this use case nor designed with the accommodation needs of such protocols in mind.

As far as Circuit Bandwidth is concerned, the proposed circuit design covers all the frequencies from 0.1 Hz to 20 kHz, and the bibliographies state that an EEG signal may appear for performing raw EEG data acquisition and artifact removal. More specifically, the proposed circuit is tested to be more than sufficient to process the EEG signal in the wavebands of particular interest in the zone of 4 Hz to 30 Hz. On the one hand, Cases "1" and "3" are designed to collect signals with frequencies from the alpha, beta, delta and theta wavebands, and they do so efficiently. From the previous two, Case "1" has a greater margin for errors, in terms of the higher cut-off frequency of the low pass filters. On the other hand, Case "2" has such a large bandwidth that it is of no use for the accurate collection of the EEG signal, thus resulting in the collection of unnecessary high frequency noise that would possibly be present in its output signal.

Finally, considering signal quality, all circuits have excellent gains for the respective use cases, with Case "2" having the strong advantage that it possesses the ability for programmable gain. In this work, this was a characteristic that was not a priority to be used in the present study, but programmable gain will be one of the design priorities in future iterations of this circuit, that are worked upon by the authors. As far as noise is concerned and its effect on signal quality, Case "2" has the best performance, with the proposed circuit design being second but in close proximity with the first in noise performance. In both cases, the noise level is acceptable. Case "3" chose a non-standard format for presenting their result, and accordingly, it cannot be directly compared with the other cases. However, it can be stated that errors pre-amplification at a level of around 1% are acceptable for certain types of applications. The use of this circuit should be contained only in those cases that are stated in the respective paper, if the user wants guarantees of accuracy in the signal acquisition process. Case "1" did not provide relevant information for the noise level. Lastly, Case "1" and the proposed novel design of this study achieve the same notch depth, while Case "3" does not state notch depth data, and Case "2" does not perform notch filtering at all. The simulation results and comparison between Cases ''1'', ''2'' and ''3'' with the proposed circuit design are presented in Table 5.

Table 5. Requirements and Specifications results comparison of the performed simulations.

Requirements/ Specifications	**Case "1"**	**Case "2"**	**Case "3"**	**Proposed Circuit EEG Design**
Common Mode Rejection Ratio (CMRR)	>120 dB	140 dB	Estimated at 110 dB	Greater than 90 dB below 110Hz
Circuit Bandwidth	0.3 to 40 Hz	3.5 MHz	0.5 to 33.86 Hz	0.5 Hz to 48kHz min (0.5 Hz to 21kHz min 0 dB passband)
Signal Quality (Gain and Noise)	▪ Gain: 25000 V/V ▪ Noise: absence of noise data ▪ Notch depth: 48 dB at 50Hz	▪ Gain: variable 40.9K to 10580K V/V ▪ Noise: Vpp noise in 0.1 Hz to 10Hz is 50nV before amplification ▪ Notch depth: -	▪ Gain: 64000 V/V ▪ Noise: pre-amplification error: 0.74% ▪ post-amplification error: 1.75% ▪ Notch depth: absence of depth data	▪ Gain: 300 V/V ▪ Noise: Vpp noise in 0.1 Hz to 10Hz is 1.4887μVrms before amplification ▪ Notch depth: 48 dB at 50Hz

At this point, a comparative analysis of Cases ''1'', ''2'' and ''3'' will be conducted in contrast with the proposed Circuit Design Innovations. Specifically, the Proposed Circuit EEG Design has a

Preprints.org (www.preprints.org) | NOT PEER-REVIEWED | Posted: 3 June 2024 doi:10.20944/preprints202404.2023.v2

series of innovations that overcome the various limitations observed. Starting this analysis with notch filtering, the proposed design has the ability to perform notching either at 50 Hz or 60 Hz, depending on the environment that the circuit is intended to be used in. Cases "1" and "3" accommodate only 50Hz EMI noise removal, and Case ''2'' does not perform any kind of notch filtering at all. Additionally, the protection of sensitive EEG electronics from static electricity is not incorporated in Cases ''1'', "2" and '3'', in contrast with the ESD protection subcircuit of the proposed design. Moreover, Cases ''1'', "2" and '3'' have not been tested in conditions with the presence of strong muscle artifacts, while the proposed design is meticulously tested for handling artifacts of such nature. It is worth mentioning the fact that Cases ''1'', ''2'' and ''3'' have not been tested for compliance with the current safety standards, making their real-world usage potentially unsafe for human use. On the contrary, the proposed circuit is in accordance with the medical device standards for EEG user patient's safety with respect to leakage current levels. Last but not least, in Cases ''1'' and ''3'', the input data with which their respective circuits were simulated are unknown, and in Case ''2'' even though the input data are clearly provided, they are rather ideal non-realistic EEG waveforms, and with certainty, do not contain compound muscle movement artifacts. In this study, a highly detailed circuit model of the Human Body and of the EMI that affects the body originates from the surrounding environment. Thus, the input data are transparently generated from the aforementioned modeling circuit, making the simulation results reproducible and reusable. Besides creating the previous asset, the proposed circuit model was adjusted to produce input data that contained muscle movement artifacts. Those generated artifacts were used to confirm the proposed circuit is capable of being used to collect raw EEG signals accurately in protocols that contain strong muscle movement. The examination of the limitations of the Cases ''1'', ''2'' and ''3'' and the proposed design innovations are thoroughly presented in Table 6.

Table 6. Examination of Cases Limitations and Proposed Design Innovations.

Circuits Comparison	Case ''1'' Limitation	Case ''2'' Limitation	Case ''3'' Limitation	Proposed Circuit EEG Design Innovation
Point of interest	▪ Notch only at 50Hz not 60Hz,	▪ No Notch at 50Hz or 60Hz,	▪ Notch only at 50Hz not 60Hz,	▪ Notch either at 50Hz or 60Hz, depending on the environment
	▪ No test for strong muscle artifacts	▪ No test for strong muscle artifacts	▪ No test for strong muscle artifacts	▪ sufficient muscle artifacts handling
	▪ No ESD protection	▪ No ESD protection	▪ No ESD protection	▪ ESD protection
	▪ Not test for compliance with the safety standards for current	▪ Not test for compliance with the safety standards for current	▪ Not test for compliance with the safety standards for current	▪ Compliance with the safety standards for current
	▪ Not input test data provided	▪ input test data provided but no data with compound muscle movement artifacts.	▪ Not input test data provided	▪ Complete Human Body and EMI simulation ▪ Test with data with compound muscle movement artifacts.

 doi:10.20944/preprints202404.2023.v2

5. Discussion

5.1. Observed Limitations of the Proposed EEG Circuit Design

The present single-channel arrangement of the EEG circuit presents a limitation, if a complete study of brain activity is desired, as it allows a very limited amount of data to be collected. Even though the design is modular and can be expanded for multichannel acquisition, this was not performed in this study. This circuit was designed as a proof of concept for efficient modeling of the electronic behavior of the brain, muscle artifacts and EMI, as well as the circuit topology needed for muscle artifacts removal during the EEG signal acquisition process. This problem can only be resolved by designing a multi-channel system that would allow simultaneous monitoring in several brain areas, an attribute that is certainly required for carrying out comprehensive neurological studies. Also, the multichannel approach could give more flexibility in muscle artifact removal, as this type of artifact is mostly a common mode signal and having better space sampling of this signal means it can be more effectively filter with hardware of software solutions.

In addition, the absence of a wireless technology MCU and ADC topology being intergraded with this circuit limits the ability of this study to be a complete proof of concept for effective EMI and muscle artifact removal in potential mobile monitoring applications. Even though the signal generator can be a step towards the verification of the reproducible simulated evaluation of EEG AFE circuits, the utility of such circuits for real time mobile EEG muscle artifacts free signal acquisition can be assessed only with the inclusion of wireless communication modules, ADCs and MCU, in order to produce a complete EEG circuit that can be tested initially in a lab environment and ultimately in real-life scenarios.

There are also concerns over the continued reliance of the circuit on battery power, which could affect the long-term operational stability and long-term efficiency in power management. Integration of resilient material and application specific battery technologies can prove highly effective in reducing the risk of single points of failure, a critical factor in decreasing the risks to medical safety regulation. To avoid this, the proposed AFE should be subjected to thorough testing within various environmental conditions, such as low, freezing and high temperatures and humidity levels, which was not part of the present study. The present AFE was not simulated if it is durable enough for use in everyday harsh weather conditions, including even a device that is waterproof.

The current study has not entertained the possible hardware choices of more advanced methods for noise reduction, such as adaptive filtering, which may be necessary for effectively responding to environmental noise, particularly from highly interfering environments like hospitals or clinics. The latter could be also addressed by incorporating enhanced electromagnetic interference (EMI) shielding in the design stage of the printed circuit board (PCB). Also, the shielding of the cables, a topic that was not part of this study is of extreme importance when designing the interface between the AFE and the electrodes that acquire the brain signals of the potential users of an EEG or BCI that could potentially use the proposed circuit as an AFE. Additional, problems of data encryption or secure data transfer were not part of this study, yet both are paramount to secure the data of patients in medical applications. Nonetheless, this is a problem that is mostly addressed by the circuitry of the MCUs incorporated in the EEG circuits and not of the AFE design. Lastly, the design was not assessed if it is in compliance with all the existing international regulatory norms in the domain of EEG, but only with those related to safety and leakage currents. This can limit it from being in place to be considered for use in any medical environment, before more studies are conducted.

5.2. Future Perspectives: Possible Updates and Real-World Applications of the Proposed EEG Circuit Design

The proposed novel EEG AFE was designed with the goal of being able to be incorporated in multi-component EEG signal acquisition systems for neurofeedback training and BCI applications. It can ensure the collection of full-brain activity in the site, where the electrode of the single channel is applied, thus facilitating better control accuracy and more efficacious neurofeedback [59].

In a future study, adaptive filtering methods combined with commercially available ADCs and microcontrollers could allow the study of the real-time data collection capabilities of the proposed

 doi:10.20944/preprints202404.2023.v2

AFE, as part of a complete system. The transmission of the acquired signal could be materialized with the use of BLE or Wi-Fi to a computer for real-time mobile BCI applications. Extending the design based on the proposed AFE for mutli-channel data acquisition is a self-evident next step for research. This will further increase spatial resolution in EEG data and can be combined with the use of highly-sensitive dry or wet electrodes and well shielded cables for minimal noise signal propagation between the electrodes and the AFE. A PCB design with meticulous care for signal integrity and avoidance of EMI is also a valid future perspective of the presented research.

Furthermore, the design of a proof-of-concept BCI application using this AFE could be also a logical next step for extending the results of this research. This BCI could also take into account hardware problem related to the AFE that arise when the designer wants to enable user-specific calibration utilities in the circuit level, such as the use of case specific Programmable Gain Amplifiers gain adjustment, based on input impedance measurements during usage. Lastly, a study on the choice of material with respect to preserving signal integrity while not minimizing signal accuracy could be a future topic of expansion of the present study.

In recapitulation, the materialization of all the above proposition translate to a more robust AFE design that would allow for cost-effective multi-channel deployments and that could be crafted for compliance with all the legal medical requirements standards for the purpose of ensuring usability in medical settings. Fixing these technological bottlenecks and having the suggestions in mind during the designing process, shows that the EEG systems could experience potential improvements for uses in research and therapeutics. This will lead to high usability and effectiveness in real-world applications. Allowing for scientific community access to the proposed ideas and concerns posed by this study could hopefully accelerate the process of reproducible AFE designs that support real-time EMI and muscle artifacts removal.

6. Conclusions

This study introduces a novel EEG Analog Front End Circuit System, distinctively capable of monitoring theta, alpha and beta brain wavebands during challenging complex EEG usage protocols involving strong compound muscle movements. This capability, which is rarely studied in the field to our best knowledge, addresses a significant gap in existing EEG technologies.

It is worth noting that by making the system capable of handling significant muscle artifacts manipulation in raw EEG data, EEG analysis becomes more accurate and reliable. Taking into consideration the effects of environmental electromagnetic interference, our project presents an unprecedented development of a realistic electronic model of the human body and brain, which can handle 50 Hz or 60 Hz power grid EMI. More importantly, the GIGO problem must be minimized when evaluating such systems. Accurate, realistic and coherent input signals are needed for system evaluation, and this requirement can be achieved through advanced input signal modeling. Our approach, which maintains the consistency, accuracy and reliability of our simulation testing, is essential for increasing the credibility and efficiency of the projected EEG.

The suggested circuit's primary characteristic is its high mobility, which is facilitated by a battery-powered configuration, allowing for application in a variety of scientific and industrial contexts. It covers a broad frequency spectrum, beginning with 0.5 Hz and reaching 48 kHz as the minimum contour's frequency. The 0 dB passband ensures a comprehensive compilation of all EEG signals, which falls within 0.5 Hz and 21 kHz. With the high amplification factor of 300 V/V, the signal may increase the signal amplitudes of EEG numerous times, and its high amplifications do not result in signal distortion. Furthermore, low levels of noise production, with a value of 1.58871 μVrms, ensure that the noise levels before amplification ranged between 0.1 Hz and 10 Hz are extremely low.

Significantly enhancing the clarity and quality of raw EEG signal readings can be achieved by reducing noise levels and attaining a 48 dB notch depth at the correct frequency. The idea shows its potential for global acceptability by mitigating Electromagnetic Interference at frequencies of either 50 Hz or 60 Hz, depending on the particular power grid configurations in the region. The circuit follows EEG design principles by achieving a High Common Mode Rejection Ratio above 90 dB when subjected to EEG signals under 110 Hz in 60 Hz EMI environments and under 166 Hz in 50 Hz EMI

 doi:10.20944/preprints202404.2023.v2

environments. The design complies with the medical equipment set requirements with respect to current levels and leakage current to ensure patient safety. Furthermore, the integration of a subcircuit specifically engineered to mitigate the risk of Electrostatic Discharge amplifies the system's robustness and durability.

To recapitulate, the aforementioned attributes lead to the production of results that are almost of medical caliber while necessitating a few electrical components. Importantly, the system retains its cost-effectiveness advantage by employing simple and minimal sub-circuits, deliberately avoiding complex and expensive techniques, and maintaining the cost close to commercial and research-grade device levels. In summary, the system's capabilities are extensively validated through carefully crafted simulations, and its potential usage extends to advanced applications such as neuro-feedback training and tele-controlling devices via Brain-Computer Interfaces, particularly in usage protocols, where the novel device’s users perform strong compound muscle movements.

 doi:10.20944/preprints202404.2023.v2

Author Contributions: Conceptualization, A.D.; methodology, A.D.; software, A.D.; validation, A.D., G.T. and P.T.; formal analysis, A.D.; investigation, A.D.; resources, A.D., and P.T.; data curation, A.D., and P.T.; writing—original draft preparation, A.D. and G.T.; writing—review and editing, A.D., G.T. and P.T.; visualization, A.D. and G.T.; supervision, P.T.; project administration, A.D. All authors have read and agreed to the published version of the manuscript.

Funding: This research received no external funding.

Institutional Review Board Statement: Not applicable.

Informed Consent Statement: Not applicable.

Data Availability Statement: The original contributions presented in the study are included in the article.

Conflicts of Interest: The authors declare no conflicts of interest.

Appendix A

This Appendix provides supplemental information for an in depth introduction to the domain of EEG circuit design techniques and requirements, the nature of the EEG signals and artifacts as well as additional information about the subcomponents of a Generic EEG circuit Template.

EEG plays a vital role in patient real-time monitoring due to its non-invasive nature in tracking brain activity. For the purpose of diagnosing neurological disorders, evaluating cerebral functioning, measuring the effectiveness of therapy, tracking the course of the disease, and providing prognostic insights, high temporal resolution is crucial. It additionally functions well as a monitoring tool during surgery and can be easily integrated with other methods such as fMRI and fNIRS.

The detail of classification of brainwave signal and their characteristics is presented in the Table A.1

Table A1. EEG Signals Categorization by Significance and Key Topics.

Frequency Band	Significance	Key Topics
Delta (0.5-4 Hz)	Deep Sleep, Unconsciousness	Basics and Beyond, Significance in Sleep and Memory, Methods, and Applications
Theta (4-8 Hz)	Creativity, Meditation, Drowsiness	Bridging Consciousness, Thalamic Origins, Practical Insights
Alpha (8-13 Hz)	Relaxation, Calmness, Decreased Attention	Indicators of Visual Activation, Enhancing Techniques and Benefits
Beta (13-30 Hz)	Active Thinking, Focus, Anxiety	Association with Alertness, Analysis to Application
Gamma (30-100 Hz)	Higher Mental Activity, Perception, Consciousness	Cognitive Functions, Exploring High-Frequency Bands

Table A.2 provides a otherview of the noises that contaminate the EEG signals and their characteristics, impact and mitigation measures [10,11].

Table A2. Noise Interference in EEG Signal Acquisition.

Type of Noise	Frequency Range	Source/Characteristics	Impact on EEG Signal	Mitigation Measures
Hardware Noise (DC)	0 Hz (DC)	Originates from wiring and electrical components of the recording system	Values up to a few μV	Use of special gear for noise reduction/isolation

 doi:10.20944/preprints202404.2023.v2

Type of Noise	Frequency Range	Source/Characteristics	Impact on EEG Signal	Mitigation Measures
Muscle Noise	0-200 Hz (1-50 Hz most impactful)	Caused by muscle activity, including minor movements like eye blinking	Values may exceed 100 mV	Careful electrode installation, skilled operators for reduction
Motion, Breath, Sweat and Cardiac Noise	0-1.2 Hz	Due to normal physical activities	Values may reach 10-80 μV	Proper installation and setup
Eye Motion & Electromagnetic Field Noise	0-16 Hz	Eye motion and intensity of electromagnetic fields	Values between 50-100 μV	Correct electrode placement, skilled operators
Electromagnetic Interference (EMI) & Circuit Noise	50 Hz (e.g. Greece), 60 Hz (e.g. USA)	From electrical power lines and nearby electronic devices	Significant distortion possible	Use of special filters for isolation

Table A.3 presents a structured overview of the various components involved in EEG circuits, along with their respective functions [12–14].

Table A3. Components involved in EEG Circuits Design (Generic).

Category	Subcomponent	Function Description
Filter	Notch Filter	Eliminates power line interference, typically at 50 or 60 Hz.
	Anti-Aliasing Filter	Prevents aliasing by removing high-frequency components before analog-to-digital conversion.
	High Pass Filter	Removes low-frequency components, typically below 0.1 Hz.
	Low Pass Filter	Cuts off frequencies higher than a certain threshold to remove high-frequency noise.
Circuit	Chopper Circuit	Reduces low-frequency noise and drift in DC amplifiers by modulating and demodulating the input signal.
	ESD Protection Circuit	Protects sensitive EEG electronics from static electricity.
Amplifier	Operational Amplifier (Op-Amp)	Amplifies the EEG signal with high gain and stability.
	Programmable Gain Amplifier	Allows for adjustment of the amplification level of the EEG signal.
	Instrumentation Amplifier with Integrated Filter	Provides high input impedance, and low noise, and includes integrated filters for signal conditioning.
Other Subcomponents	Analog Mux (Multiplexer)	Selects one of several input signals and forwards it into a single line in multi-channel EEG systems.
	Analog to Digital Converter (ADC)	Converts the analog EEG signal into a digital format for processing and analysis.
	Drive Right Leg Circuit	Reduces common-mode interference in biopotential amplifiers.

The technical distinctions in design specifications between medical-grade and research-grade EEG circuits [22] are illustrated in Table A.4.

 doi:10.20944/preprints202404.2023.v2

Table A4. Comparison of the Key Technical Aspects of Medical-Grade & Research-Grade EEG Circuits.

Aspect	Medical-Grade EEG	Research-Grade EEG
Accuracy and Resolution	Higher accuracy and resolution for diagnostic purposes	Slightly lower resolution, suitable for studying brain patterns
Number of Electrodes	Higher number, standardized layouts (e.g., 10-20 system)	Fewer electrodes, focusing on specific brain regions
Signal Quality and Noise Reduction	Advanced noise reduction for highly accurate readings	Noise reduction present, but may prioritize flexibility in analysis
Regulatory Compliance and Certification	Must meet strict regulatory standards (e.g., FDA approval)	Not subjected to the same level of regulatory scrutiny
Durability and Robustness	Designed for frequent and sustained use, more durable	May not be as durable, focuses on flexibility for research

Appendix B

This Appendix provides an overview of the EEG circuit designs analyzed in this study. It delineates the requisite parameters and technical specifications for some of the circuits that are not part of the direct comparison with the proposed EEG Circuits and the distinct Cases ‘’1’’, ‘’2’’, and ‘’3’’, as well as more details about Cases ‘’1’’, ‘’2’’, and ‘’3’’.

B.1. Supplementary information for Case “1”

B.1.1 Comparative Evaluation with EEG Generic Circuit Design

The comparison of the low-cost EEG circuit design with the aforementioned generic model in this study underscores the novel aspects of combining multiple filters and amplifier stages. This design is characterized by ease of implementation because advanced design techniques are avoided (e.g., chopping), robust anti-interference capabilities are achieved by the high-pass filters, and high signal amplification from the amplifier is guaranteed by two instead of one amplification stage.

B.1.2. Usage-Centric Justification for Design Differentiation: Case "1"

The definition of a low-cost EEG circuit design provides real-time, high-quality, and cost-effective signal processing specifically designed to support the development of advanced Brain-Computer Interface systems (BCI). It is very good in precisely enhancing and optimizing raw EEG signals. In addition, it could serve as a portable detector for EEG signals in a research or medical environment. These features have proved to be high input resistance, high CMRR, high gain, large gains, substantial, low noise, low drift currents, low drift currents, low-frequency response, and substantial estimated SNR.

B.1.3. Simulation - Experimental Results: Case "1"

These experimental results, therefore, indicate that the design of the low-cost EEG circuit can be used for signal extraction and amplification. This further will confirm that the design can maintain stability and performances of the circuits while enhancing the EEG signal, dropping the low frequency, and reducing the power line interference. According to the research of Case "1," it is noted that this assessment is very important and significant, since it will emerge if the design of the project meets the requirements and, on top of that, it will reflect on the development of EEG circuits.

 doi:10.20944/preprints202404.2023.v2

B.2. Supplementary information for Case "2"

B.2.1. Comparative Evaluation with EEG Generic Circuit Design

This study demonstrated the uniqueness of the low-noise, battery-operated EEG amplifier system that has simple filtering in comparison with the Generic model. As a result, this system posts an exact instrumentation and inverting amplifier to come out with minimal design while consuming low power for sustainability and portability, since it's battery-operated. It also includes superior CMRR and SNR for accurate amplification and reliable readings, high input impedance to prevent signal distortion, and high gain for clear signal interpretation. While it has a low-pass filter to remove high-frequency noise, it deliberately lacks a notch filter. This is attributed to the fact that it is not connected to supply from the main grid, but still, a notch filter could have been of use for tackling EMI from the main grid . Consequently, it can be used to identify neurological irregularities, demonstrating its effectiveness in advanced neurological research.

B.2.2. Usage-Centric Justification for Design Differentiation: Case "2"

Further, the design of this biomedical device is in consideration of low power consumption; as such, this design befits the requirement for use in most cases of research that will see a long time in practical use. Or even better, the quality of acquired EEG signals is even higher when using a battery to reduce noise from the electric grid and increase the strength of the device because it will, therefore, last longer. Therefore, this circuit is a fine candidate for use in setting up the research protocols where portability, low noise, and low cost of the device are the major issues to be considered.

B.2.3. Simulation - Experimental Results: Case "2"

Results in this study supported and established the role of the tested device, the low-noise battery-powered amplifier, in signal isolation and amplification. In this context, the results validate the ability for accurate records of EEG signals and hence the usefulness of the device in ascertaining a number of research protocols. The asset of low energy usage, the minimally flexible design, and the portability of the BB-ESAS extend its applicability in both home-use and research settings. Nonetheless, the simulation was conducted only with EEG signals of one wave band at a time in the total absence of noise (a nonrealistic signal of brain physiology). This simulation setting makes the usage of this EEG circuit questionable when it is operated in high-EMI environments or in protocols with strong compound muscle movements. Last but not least, this system, though it removes noise from low-amplitude EEG signals, does not handle low-frequency drift and does not involve necessary ESD protection.

B.3. Supplementary Information for Case "3"

B.3.1. Comparative Evaluation with EEG Generic Circuit Design

The comparison between the dual-notch filter EEG circuit design and the generic one emphasizes the essential variables that contribute to Case ''3'' circuit's superior performance. This design has the novelty of 1 pre-amplification and 2 amplification stages. In addition, the way in which electrodes are attached to the scalp provides a low-impedance path to achieve minimal common mode interference noise contained in the signal coming from the body. As a result, this eliminates the requirement for protective electric shielding when collecting EEG signals. Moreover, this circuit configuration employs a rare (unorthodox) engineering decision by using two-notch filters, which greatly improves the suppression of electromagnetic interference originating from the power grid.

B.3.2. Usage-Centric Justification for Design Differentiation: Case "3"

First, it is applicable for the clinical diagnoses over fine monitoring of brain diseases with accuracy since it does not require electrical shielding technology, the EEG. The configuration is hence mandatory in the medical settings for proper diagnosis and treatment effectuality. This EEG technology has further important uses: in national defense and aerospace medicine. The industries

 doi:10.20944/preprints202404.2023.v2

served by the medical units require systems that are both sturdy and flexible. Most of these systems are easily prone to a host of electromagnetic interference (EMI) sources, including: The human body is biologically eliminated through the use of pre-amplification techniques, driven-right-leg circuits, and biomedical engineering. Such decisions in the design help the effective detection of the EEG signals in environments that lack proper shielding. This development, therefore, significantly eases the logistic problems the conventional methods of data collection in EEG have and, therefore, reduces these constraints for Case '3', making them much more feasible and accessible for their implementation in a wide variety of contexts. A brain-computer interface (BCI) device retrieves the signals of EEG. As such, where accuracy of such brain activities is very much necessary, to assure reliability in the systems, this circuit would facilitate essential signal recording.

B.3.3. Simulation - Experimental Results: Case "3"

The experimental output of this specific EEG signal amplifier is demonstrative of its utility to isolate noise and enhance signals effectively. The high CMRR of the main amplifier, the ability to eliminate high-frequency noise and 50Hz frequency interference, and a gain of more than 60,000 V/V produce a low-noise, significantly amplified analog signal that is excellent for digital conversion. This EEG circuit design, by using the pre-amplifier and post-amplifier, along with high-performance filter sets (two low-pass filters and two 50Hz traps), has high performance in effective amplification and extraction, which can be achieved in non-shielded environments, potentially expanding the range of applicability of EEG systems.

B.4. Supplementary Information for Four other Circuits of Related Works

The following Table B1. succinctly presents key aspects of the Neonates-Specific EEG System [43], including the CMRR, signal bandwidth, gain, and filter characteristics:

Table B1. Parameters and technical specifications in Neonates-Specific EEG System.

Feature	Description
Common Mode Rejection Ratio (CMRR)	The AD620 instrumentation amplifier used in the design has a high CMRR of 110 dB, crucial for minimizing noise and interference in EEG signals.
Signal Bandwidth/Frequency Range	Targets neonatal EEG signals, predominantly delta waves, with frequencies from 0.5 to 2 Hz, 100µV amplitude.
Gain	Total gain of 17776 V/V. Individual stage gains: ▪ 16 V/V (instrumentation amplifier), ▪ 101 V/V (second stage), ▪ 11 V/V (third stage).
Filter Characteristics	High pass and low pass filters with cutoff frequencies of 0.16 Hz and 50 Hz, respectively to remove DC offset and power line interference

The following Table B2 provides a succinct overview of the compact amplifier and signal conditioning module designed for wireless EEG monitoring [44]. This kind of EEG design includes features, relate to variable gain, CMRR, power consumption, portability, components, cost, and signal quality metrics. The design prioritizes low power consumption and portability, utilizing readily available commercial components to achieve a cost-efficient and compact solution.

 doi:10.20944/preprints202404.2023.v2

Table B2. Wireless EEG Monitoring-Compatible Compact Amplifier and Signal Conditioning Module.

Feature	Description
Common Mode Rejection Ratio (CMRR)	High CMRR suitable for EEG applications
Signal Bandwidth	0.5 to 40 Hz
Variable Gain	Between 100 and 7000
Power Consumption	Low
Portability	Designed for portability
Components	Uses commercially available components
Cost	Cost-effective
Signal Quality Metrics	Detailed metrics not directly provided

The following Table B3 systematically organizes the technical parameters of a Single-Chip EEG Signal Sampling Circuit [45], such as Common Mode Rejection Ratio (CMRR), Amplifier Gain, Pass-Band Frequency, and Input Impedance:

Table B3. Single-Chip EEG Signal Sampling Circuit.

Feature	Description
Common Mode Rejection Ratio (CMRR)	102 dB, effective in reducing noise and interference from common-mode signal
Amplifier Gain	Variable, with options for 5000, 10000, 20000, or 30000 V/V
Pass-Band Frequency	Ranges from 0.12Hz to 35.4Hz, accommodating the typical frequency range of EEG signals
Input Impedance	113MΩ, ensuring that the circuit does not significantly load the signal source, preserving signal integrity

The following Table B4 offers a concise summary of key BCI-Specific EEG [46,60] design elements, such as CMRR, amplifier gain, notch filter, etc. These elements highlight the circuit's ability to deliver accurate amplification and filtering of EEG signals, which are crucial for dependable monitoring of brain activity:

Table B4. BCI-Specific EEG.

Feature	Description
Common Mode Rejection Ratio (CMRR)	100 dB for gains ≥ 100, aiming for effective common-mode noise rejection
Amplifier Gain	G≥100V/V
Modified High-Q Factor Active Twin-T Notch Filter	60 Hz and a rejection level of -38 dB.
PCB Size	Less than 5.5 cm2

Appendix C

This has all the supplementary images, equations and calculations that accompany the Material and Methods Section of this work.

Figure C.1 depicts the EEG sub-circuit modeling the EMI in a 50 Hz electric grid.

Preprints.org (www.preprints.org) | NOT PEER-REVIEWED | Posted: 3 June 2024 doi:10.20944/preprints202404.2023.v2

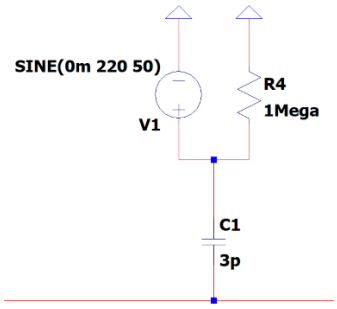

Figure C.1 EEG Sub-Circuit Modeling the EMI in 50 Hz Electric Grid.

In Figure C.2, the EEG sub-circuit modeling the human body apart from the brain during protocols with strong compound muscle movement is depicted.

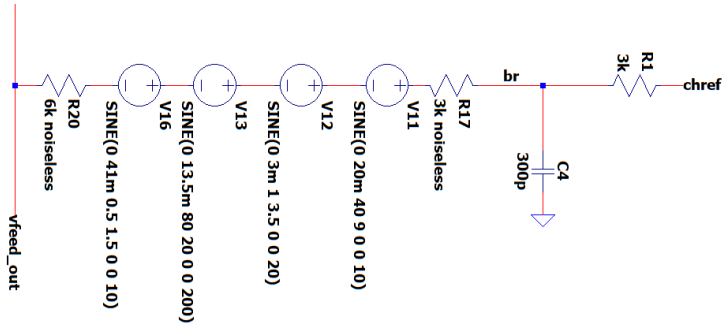

Figure C.2. EEG Sub-circuit Modeling the Human Body Apart from the Brain.

In Figure C.3 is depicted the EEG sub-circuit modeling the brain and the electrode.

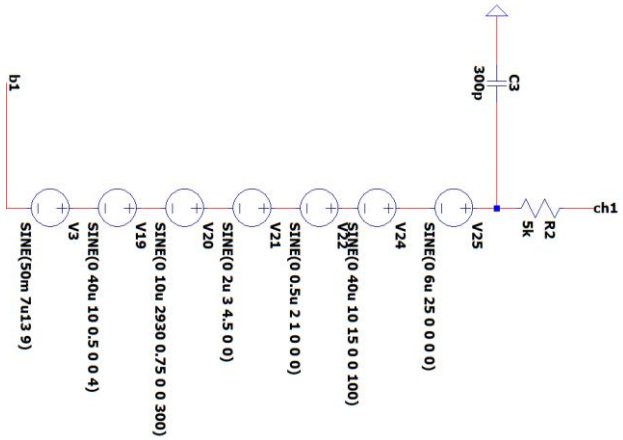

Figure C.3. EEG sub-Circuit Modeling the Brain and the Electrode.

In Figure C.4, the EEG sub-circuit is depicted, modeling the battery supply of the system.

Preprints.org (www.preprints.org) | NOT PEER-REVIEWED | Posted: 3 June 2024 doi:10.20944/preprints202404.2023.v2

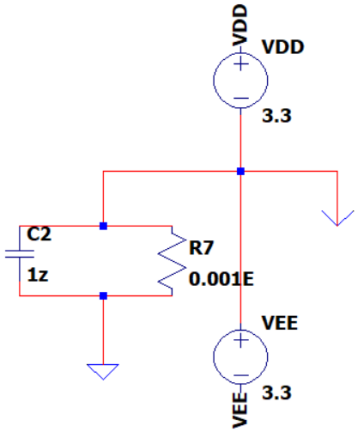

Figure C.4. EEG Sub-Circuit Modeling 3.3V Battery Supply.

In Figure C.5 is depicted the EEG sub-circuit modeling the driven right leg circuit.

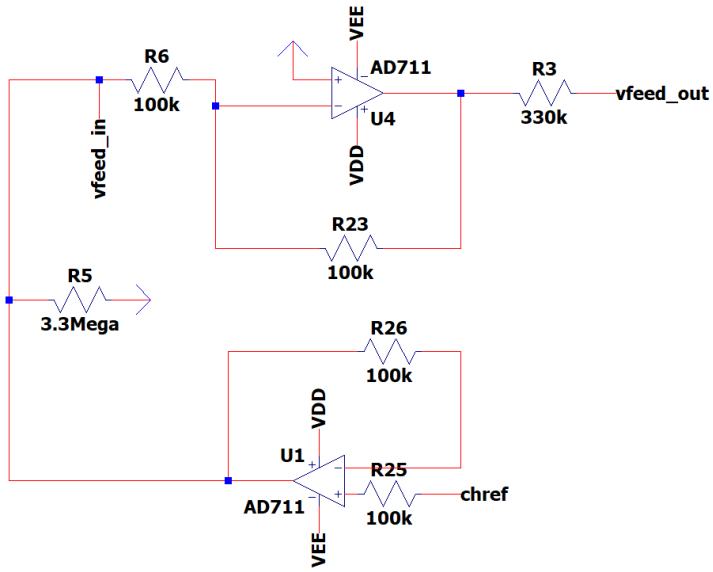

Figure C.5. EEG Sub-Circuit Modeling the DRL Circuit.

With respect to the first band-pass filter, it exhibits a Q factor of 0.0014854, a damping ratio of ζ = 336.598, and a center frequency of 324.6667 Hz under the condition that the input resistance is 331 KΩ. The filter exhibits a Q factor of 0.0033969, a damping ratio of ζ = 147.191, and a center frequency of 141.972 Hz under the condition that the input resistance is 1731 KΩ. The considerations described above result in minimal phase distortion within the acceptable frequency range for our amplification needs. The system takes around 30 msec to reach 99.99% of its final value. The equation describing the circuit above is:

$$f_{3db} = s * \frac{\frac{1}{Rf11*Cf11}}{s^2+s*\left(\frac{1}{Rf12*Cf12}+\frac{1}{Rf11*Cf12}+\frac{1}{Rf11*Cf11}\right)+\frac{1}{Rf12*Cf12*Rf12*Cf12}} \quad \text{(C.1)}$$

In Figure C.6 is depicted the EEG sub-circuit modeling the first band-pass filter

Preprints.org (www.preprints.org) | NOT PEER-REVIEWED | Posted: 3 June 2024 doi:10.20944/preprints202404.2023.v2

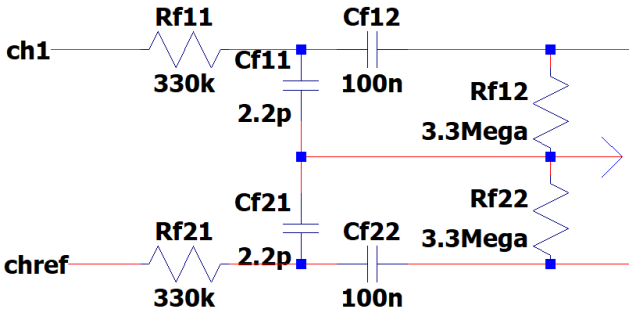

Figure C.6. EEG Sub-Circuit Modeling the First Band-Pass Filter.

With respect to the instrumentation amplifier, the equation describing the instrumentation amplifier's gain is:

$$G = 1 + \frac{19.8\ \text{k}\Omega}{R_G} \tag{C.2}$$

In **Figure** C.7 is depicted the EEG sub-circuit modeling the ESD protection and the instrumentation amplifier.

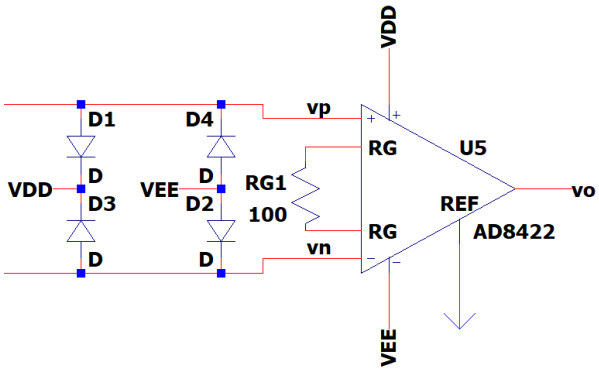

Figure C.7. EEG Sub-Circuit Modeling the ESD Protection and the Instrumentation Amplifier.

With respect to the notch filter, the equations governing the center frequency f_o and Quality factor Q are [35]:

$$f_o = \frac{1}{2\pi R_O C_O} \tag{C.3}$$

$$Q = \frac{R_Q}{2R_O} \tag{C.4}$$

In the case of the 50Hz grid the (C.3) and (C.4) yield a center frequency and Quality factor of:

$$f_o = \frac{1}{2\pi R_O C_O} = \frac{1}{2\pi * (3 * 10 + 2 * 33)\text{k}\Omega * 33nF} = \frac{1}{2\pi * 96\text{k}\Omega * 33nF} \approx 50.2383\ \text{Hz}$$

$$Q = \frac{R_Q}{2R_O} = \frac{4.7\text{M}\Omega}{2 * (3 * 10 + 2 * 33)\text{k}\Omega} = \frac{4.7\text{M}\Omega}{2 * 96\text{k}\Omega} \approx 24.4791$$

respectively.

Preprints.org (www.preprints.org) | NOT PEER-REVIEWED | Posted: 3 June 2024 doi:10.20944/preprints202404.2023.v2

In contrast, we employ the 33 kΩ resistance parallel to RO6 and RO10 for the 60Hz grid. (C.3) and (C.4) yield a center frequency and Quality factor as follows:

$$\text{fo} = \frac{1}{2\pi R_O C_O} = \frac{1}{2\pi * \left(3 * 10 + 33 + \frac{33 * 33}{33 + 33}\right) \text{k}\Omega * 33nF}$$

$$= \frac{1}{2\pi * 79.5\text{k}\Omega * 33nF} \approx 60.665 \text{ Hz}$$

$$\text{Q} = \frac{\text{R}_\text{Q}}{2R_O} = \frac{4.7\text{M}\Omega}{2 * (3 * 10 + 33 + \frac{33 * 33}{33 + 33})\text{k}\Omega} = \frac{4.7\text{M}\Omega}{2 * 79.5\text{k}\Omega} \approx 29.5597$$

respectively.

In Figure C.8 is depicted the EEG sub-circuit modeling the Fliedge notch filter 50hz or 60h.

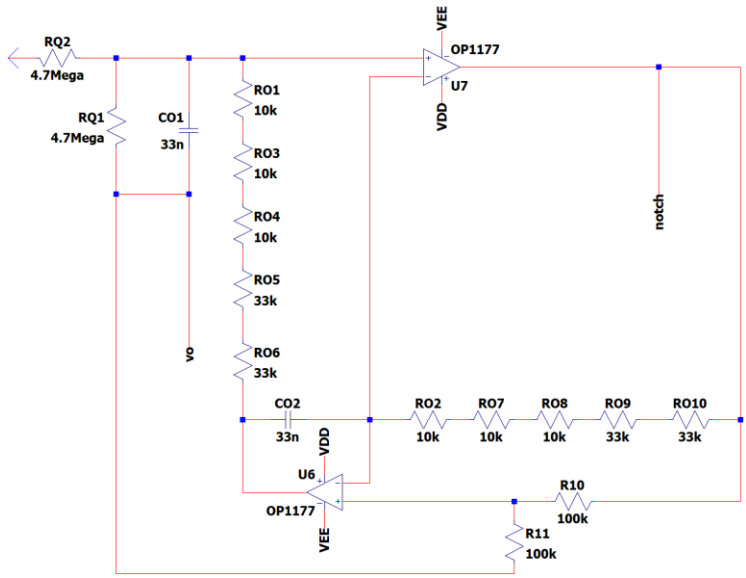

Figure C.8. EEG sub-circuit modeling the Fliedge Notch Filter 50Hz or 60Hz.

The cut-off frequency is calculated using the equation:

$$f_c = \frac{1}{2\pi R_{f31}\, C_{f31}} (5) \qquad \text{(C.5)}$$

Utilizing (C.5) in our sub-circuit design, the 3 dB cut-off frequency can be calculated as follows:

$$f_c = \frac{1}{2\pi * 330\text{k}\Omega * 22pF} \approx 48228.77\ Hz = 48.22877\ KHz$$

In Figure C.9 is depicted the EEG sub-circuit modeling the second low pass filter.

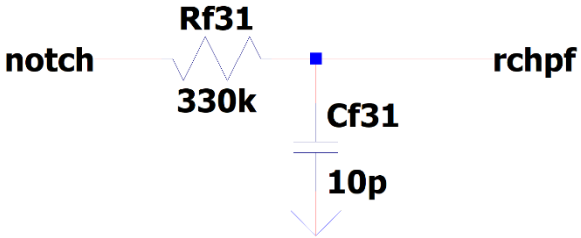

Figure C.9. EEG Sub-Circuit Modeling the Second Low Pass Filter.

Preprints.org (www.preprints.org) | NOT PEER-REVIEWED | Posted: 3 June 2024 doi:10.20944/preprints202404.2023.v2

The two important parameters that characterize the Butterworth filter are AF gain and fl cutoff -3 dB frequency:

$$A_F = 1 + \frac{R_{f42}}{R_{f41}} \tag{C.6}$$

$$f_l = \frac{1}{2\pi R_{f43}\, C_{f41}} \tag{C.7}$$

Utilizing (C.6) to our sub-circuit design, the AF gain can be calculated as:

$$A_F = 1 + \frac{R_{f42}}{R_{f41}} \approx 1.588$$

Utilizing (C.7) to our sub-circuit design, the 3 dB cut-off frequency fl can be calculated as:

$$f_l = \frac{1}{2\pi * 3.3M\Omega * 100nF} \approx 482.287\mu Hz$$

If ''f ''is the frequency of the input signal the magnitude of the voltage gain is:

$$\left|\frac{V_{out}}{V_{rchpf}}\right| = \frac{A_F * \frac{f}{f_l}}{\sqrt{\left(1 + \left(\frac{f}{f_l}\right)^2\right)}} = \frac{3.2926 * f}{\sqrt{\left(1 + \left(\frac{f}{0.482287}\right)^2\right)}}$$

In Figure C.10 is depicted the EEG Sub-Circuit Modeling the Second High Pass Filter before the Analog to Digital Conversion.

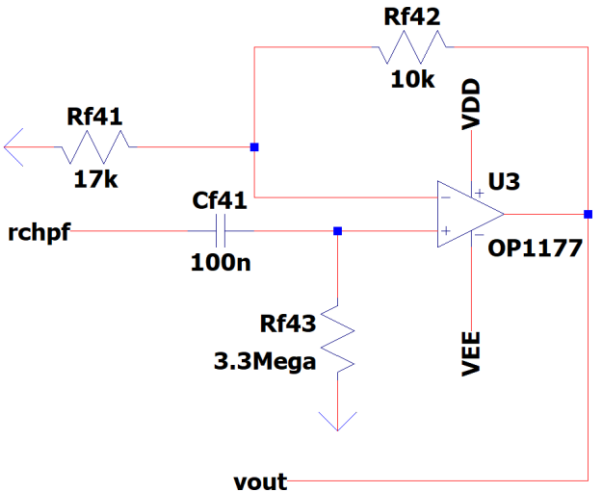

Figure C.10. EEG Sub-Circuit Modeling the Second High Pass Filter.

The noise of our design before the first amplification estimated as the total Vpp noise in the equivalent noise bandwidth range of 0.1Hz to 10Hz is given by the equation:

$$e_{nt} = e_n * \sqrt{ENBW} \tag{C.8}$$

$$e_n = \sqrt{4 * k_B * T * R} \approx 0.13 * \sqrt{R} \tag{C.9}$$

where:

- kB is the Boltzmann's constant,

 doi:10.20944/preprints202404.2023.v2

- T is absolute temperature in Kelvin in our case at room temperature (usually 25 C°) and
- R is the real part of the band-pass filter's impedance.

From (C.8) and (C.9) we calculate:

$$ENBW = 10 - 0.1 = 9.9\ Hz$$

$$e_{n1} \approx 0.13 * \sqrt{3300000} \approx 236.156\ nV/\sqrt{Hz}$$

$$e_{n2} \approx 0.13 * \sqrt{330000} \approx 74.679\ nV/\sqrt{Hz}$$

$$e_{nt1} = e_{n1} * \sqrt{ENBW} \approx 236.156 * \sqrt{9.9} \approx 743.049\ nV$$

$$e_{nt2} = e_{n2} * \sqrt{ENBW} \approx 74.679 * \sqrt{9.9} \approx 234.972\ nV$$

$$e_{nt} = \sqrt{e_{nt1}^2 + e_{nt2}^2} \approx 779.316\ nV$$

References

1. https://doi.org/10.1016/j.cub.2018.11.052
2. Chaudhary, U.; Birbaumer, N.; Ramos-Murguialday, A. Brain–computer interfaces for communication and rehabilitation. *Nature Reviews Neurology* **2016**, 12(9), 513–525. https://doi.org/10.1038/nrneurol.2016.113
3. Sanei, S.; Chambers, J. A. Fundamentals of EEG Signal Processing. *EEG Signal Processing* **2007**, 35–12. https://doi.org/10.1002/9780470511923.ch2.
4. Tatum, W. O. Ambulatory EEG. In Handbook of EEG Interpretation. Springer Publishing Company 2021.https://doi.org/10.1891/9780826147097.0007.
5. Benbadis, S. R.; Beniczky, S.; Bertram, E.; MacIver, S.; Moshé, S. L. The role of EEG in patients with suspected epilepsy. *Epileptic Disorders* **2020**, 22(2), 143–155. https://doi.org/10.1684/epd.2020.1151.
6. Rubiños, C.; Godoy, D. A. Electroencephalographic monitoring in the critically ill patient: What useful information can it contribute? *Medicina Intensiva (English Edition)* **2020**, 44(5), 301–309. https://doi.org/10.1016/j.medine.2019.06.008
7. Michel, C. M.; & Murray, M. M. Towards the utilization of EEG as a brain imaging tool. *NeuroImage* **2012**, 61(2), 371–385. https://doi.org/10.1016/j.neuroimage.2011.12.039
8. Aboalayon, K.; Faezipour, M.; Almuhammadi, W.; Moslehpour, S. Sleep Stage Classification Using EEG Signal Analysis: A Comprehensive Survey and New Investigation. *Entropy* **2016**, 18(9), 272. https://doi.org/10.3390/e18090272
9. Diykh, M.; Li, Y.; Wen, P. EEG Sleep Stages Classification Based on Time Domain Features and Structural Graph Similarity. *IEEE Transactions on Neural Systems and Rehabilitation Engineering* **2016**, 24(11), 1159–1168. https://doi.org/10.1109/tnsre.2016.2552539
10. Asadzadeh, S.; Yousefi Rezaii, T.; Beheshti, S.; Delpak, A.; Meshgini, S. A systematic review of EEG source localization techniques and their applications on diagnosis of brain abnormalities. Journal of Neuroscience Methods 2020, 339, 108740. https://doi.org/10.1016/j.jneumeth.2020.108740.
11. Dhar, P.; & Garg, V. K. Brain-Related Diseases and Role of Electroencephalography (EEG) in Diagnosing Brain Disorders. Lecture Notes in Networks and Systems, Springer Singapore 2020, 317–326. https://doi.org/10.1007/978-981-15-8354-4_32.
12. Ullah, H.; Mahmud, S.; Chowdhury, R. H. Identification of Brain disorders by Sub-band Decomposition of EEG signals and Measurement of Signal to Noise Ratio. *Indonesian Journal of Electrical Engineering and Computer Science* **2016**, 4(3), 568. https://doi.org/10.11591/ijeecs.v4.i3.pp568-579
13. Iscan, Z.; Dokur, Z.; Demiralp, T. Classification of electroencephalogram signals with combined time and frequency features. *Expert Systems with Applications* **2011**, 38(8), 10499–10505. https://doi.org/10.1016/j.eswa.2011.02.110.
14. Siuly, S.; Li, Y.; Zhang, Y. Electroencephalogram (EEG) and Its Background. *EEG Signal Analysis and Classification* **2016**, 3–21. https://doi.org/10.1007/978-3-319-47653-7_1.
15. Puce, A.; Hämäläinen, M. A Review of Issues Related to Data Acquisition and Analysis in EEG/MEG Studies. *Brain Sciences* **2017**, 7(12), 58. https://doi.org/10.3390/brainsci7060058
16. Mumtaz, W.; Rasheed, S.; Irfan, A. Review of challenges associated with the EEG artifact removal methods. *Biomedical Signal Processing and Control* **2021**, 68, 102741. https://doi.org/10.1016/j.bspc.2021.102741

17. Usakli, A. B. Improvement of EEG Signal Acquisition: An Electrical Aspect for State of the Art of Front End. *Computational Intelligence and Neuroscience* **2010**, 1–7. https://doi.org/10.1155/2010/630649.
18. Chen, X.; Xu, X.; Liu, A.; Lee, S.; Chen, X.; Zhang, X.; McKeown, M. J.; Wang, Z. J. Removal of Muscle Artifacts From the EEG: A Review and Recommendations. *IEEE Sensors Journal* **2019**, 19(14), 5353–5368. https://doi.org/10.1109/jsen.2019.2906572
19. Sanei, S. Book: *Adaptive Processing of Brain Signals.* Wiley 2013, ISBN 9781118622162 https://doi.org/10.1002/9781118622162
20. Lebedev, M. A.; Nicolelis, M. A. L. Brain-Machine Interfaces: From Basic Science to Neuroprostheses and Neurorehabilitation. *Physiological Reviews* **2017**, 97(2), 767–837. https://doi.org/10.1152/physrev.00027.2016
21. Elsayed, N.; Saad, Z.; Bayoumi, M. Brain Computer Interface: EEG Signal Preprocessing Issues and Solutions. *International Journal of Computer Applications* **2017**, 169(3), 12–16. https://doi.org/10.5120/ijca2017914621.
22. Alkhorshid, D. R.; Molaeezadeh, S. F.; & Alkhorshid, M. R. Analysis: Electroencephalography Acquisition System: Analog Design. Biomedical Instrumentation & *Technology* **2020**, 54(5), 346–351. https://doi.org/10.2345/0899-8205-54.5.346
23. Cohen, M. X. Where Does EEG Come From and What Does It Mean? *Trends in Neurosciences* **2017**, 40(4), 208–218. https://doi.org/10.1016/j.tins.2017.02.004.
24. Tankisi, H.; Burke, D.; Cui, L.; de Carvalho; M., Kuwabara, S.; Nandedkar, S. D.; Rutkove, S.; Stålberg, E.; van Putten, M. J. A. M.; Fuglsang-Frederiksen, A. Standards of instrumentation of EMG. *Clinical Neurophysiology* **2020**, 131(1), 243–258. https://doi.org/10.1016/j.clinph.2019.07.025.
25. Vanhatalo, S.; Voipio, J.; Kaila, K. Full-band EEG (FbEEG): an emerging standard in electroencephalography. *Clinical Neurophysiology* **2005**. 116(1), 1–8. https://doi.org/10.1016/j.clinph.2004.09.015.
26. Hari, R.; Parkkonen, L.; Nangini, C. The brain in time: insights from neuromagnetic recordings. *Annals of the New York Academy of Sciences* **2010**, 1191(1), 89–109. https://doi.org/10.1111/j.1749-6632.2010.05438.x.
27. Sullivan, T. J.; Deiss, S. R.; Cauwenberghs, G. A Low-Noise, Non-Contact EEG/ECG Sensor. In Proceeding of IEEE Biomedical Circuits and Systems Conference, Nov. 2007. https://doi.org/10.1109/biocas.2007.4463332.
28. Scheer, H. J.; Sander, T.; & Trahms, L. The influence of amplifier, interface and biological noise on signal quality in high-resolution EEG recordings. *Physiological Measurement* **2005**, 27(2), 109–117. https://doi.org/10.1088/0967-3334/27/2/002
29. Jobert, M.; Wilson, F. J.; Ruigt, G. S. F.; Brunovsky, M.; Prichep, L. S.; Drinkenburg, W. H. I. M. Guidelines for the Recording and Evaluation of Pharmaco-EEG Data in Man: The International Pharmaco-EEG Society (IPEG). *Neuropsychobiology* **2012**, 66(4), 201–220. https://doi.org/10.1159/000343478.
30. Wasade, V. S.; Spanaki, M. V. Understanding Epilepsy. Cambridge University Press, 2019. https://doi.org/10.1017/9781108754200.
31. Usakli, A. B. Improvement of EEG Signal Acquisition: An Electrical Aspect for State of the Art of Front End. *Computational Intelligence and Neuroscience* **2010**, 1–7. https://doi.org/10.1155/2010/630649.
32. Gardella, P. J.; Baez, E.; Cesaretti, J. M. (2020). Design of ESD protections for ECG applications. In Proceeding of Conference on Electronics (CAE), Argentine, Feb 2020. https://doi.org/10.1109/cae48787.2020.9046370.
33. Kuo, K.-C.; Chen, C.-T.; Liao, H.-Y. An Area Efficient Analog Front-End for Sensing EEG Signals with MOS Capacitors in 90nm Process. In Proceeding of International Conference on Consumer Electronics - Taiwan (ICCE-Taiwan) 2023. https://doi.org/10.1109/icce-taiwan58799.2023.10226840
34. Cornelio, Z. U.; Resurreccion, P.; Leon, M. T. de, Rosales; M.; Hizon, J. R. An EEG Analog Front-End Unit for Wearable Applications Implemented in 28nm FD-SOI. In Proceeding of 20th International SoC Design Conference (ISOCC) 2023. https://doi.org/10.1109/isocc59558.2023.10396619
35. Le, D. H.; Pham, T.-H.; Pham, C.-K. Design of a Configurable 4-Channel Analog Front-End for EEG Signal Acquisition on 180nm CMOS Process. *REV Journal on Electronics and Communications* **2023**. https://doi.org/10.21553/rev-jec.339
36. Pham, T.-H.; Huynh, H.-A.; Pham, C.-K.; Le, D.-H. Design of a Configurable Low-Noise 1-Channel Analog Front-End for EEG Signal Recording on 180nm CMOS Process. In Proceeding of International Conference on Advanced Technologies for Communications (ATC) 2023. https://doi.org/10.1109/atc58710.2023.10318515
37. Li, X.; Ren, S., Li, X.; Zhao, T.; Deng, X.; Zheng, W. An LFP/AP Mode Reconfigurable Analog Front-End Combining an Electrical EEEG-iEEG Model for the Closed-Loop VNS. *IEEE Transactions on Biomedical Circuits and Systems* **2024**, 18(2), 408–422. https://doi.org/10.1109/tbcas.2023.3333369
38. Hu, H.-Y.; Wang, L.-H.; Kuo, I.-C.; Wang, M.-H.; Wang, S.-F.; Huang, P.-C. A Multi-Channel EEG Acquisition Device Based on BT Microcontroller. In Proceeding of International Conference on Consumer Electronics - Taiwan (ICCE-Taiwan) 2023. https://doi.org/10.1109/icce-taiwan58799.2023.10227057

39. Han, Y.; Zhao, L.; Stephany, R. G.; Hsieh, J.-C.; Wang, H.; Jia, Y. A Scattered Wireless EEG Recording System. In Proceeding of IEEE Biomedical Circuits and Systems Conference (BioCAS) 2023. https://doi.org/10.1109/biocas58349.2023.10388939
40. Chen, W. Multi-channel EEG signal acquisition system based on nRF52832. In Proceeding of 5th International Conference on Communications, Information System and Computer Engineering (CISCE) 2023. https://doi.org/10.1109/cisce58541.2023.10142276
41. Liu, L.; Xu, J.; Yin, J.; Liao, X.; Tian, Y. (). A Low-Power and Constant-Bandwidth Analog Front End Based on Current-Reused DDA for Multibiosignal Acquisition. *IEEE Sensors Journal* **2023**, 23(20), 24711–24720. https://doi.org/10.1109/jsen.2023.3309392
42. Ge, T.; Li, P.; Duan, Q.; Yu, G. A low-noise, high-precision chopper instrument amplifier for EEG signal amplification. In Proceeding of 5th International Conference on Circuits and Systems (ICCS) 2023. https://doi.org/10.1109/iccs59502.2023.10367346
43. Kumar, S. C. P.; Chandrasekar, A.; Nagaraj, A.; Gupta, P.; Sekhar, S. Design of an ElectroEncephaloGram (EEG) amplification circuit for neonates. In Proceeding of International Conference on Communication and Signal Processing (ICCSP), Apr. 2016. https://doi.org/10.1109/iccsp.2016.7754542.
44. Whitchurch, A. K.; Abraham, J. K.; Lonkar, M. A.; Varadan, V. K. Design of a Compact Amplifier and Signal Conditioning Module for Wireless EEG Monitoring. In Proceeding of IEEE Region 5 Technical Conference, Apr. 2007. https://doi.org/10.1109/tpsd.2007.4380371.
45. Zhang, X.; & Zhang, Z. Design on Sampling Circuit of EEG Signal Based on AT89C2051 Single-Chip. In Proceeding of Fourth International Conference on Innovative Computing, Information and Control (ICICIC), Dec. 2009. https://doi.org/10.1109/icicic.2009.169.
46. Salahuddin Morsalin, S. M.; Lai, S.-C. Front-end circuit design for electroencephalography (EEG) signal. In Proceeding of 2nd International Conference on Computing, Analytics and Networks (ICAN), Indo – Taiwan, Feb 2020. https://doi.org/10.1109/indo-taiwanican48429.2020.9181346.
47. Xu, X.; Wang, P. Low-Cost Circuit Design for EEG Signal Amplification and Extraction. In Proceeding of IEEE Asia-Pacific Conference on Image Processing, Electronics and Computers (IPEC), Apr. 20212021. https://doi.org/10.1109/ipec51340.2021.9421325.
48. Choudhary, S. K.; & Bera, T. K. Designing of Battery-Based Low Noise Electroencephalography (EEG) Amplifier for Brain Signal Monitoring: A Simulation Study. In Proceeding of IEEE 6th International Conference on Condition Assessment Tech-niques in Electrical Systems (CATCON), 422-426, Durgapur, India, 2022). https://doi.org/10.1109/catcon56237.2022.10077655.
49. Analog Devices, Inc. AD8428: High Gain, High Voltage Instrumentation Amplifier. Data Sheet. Available online: https://www.analog.com/media/en/technical-documentation/data-sheets/ad8428.pdf (accessed on 10 Feb. 2024).
50. Yuge, Sun.; Ning, Ye.; Feng, Pan. A novel design of EEG signal amplifier. In Proceeding of 24th Chinese Control and Decision Conference (CCDC), May 2012. https://doi.org/10.1109/ccdc.2012.6244536.
51. Tsavdaridis, G.; Papaodysseus, C.; Karadimas, N. V.; Papazafeiropoulos, G.; Delis, A. Methodologies and Handling Techniques of Large-Scale Information in Decision Support Systems for Complex Missions. *Applied Sciences* **2024**, 14(5), 1995. https://doi.org/10.3390/app14051995
52. Tsavdaridis, G. Thesis: Adjustable and Adaptable Systems for Crisis Management Support, Monitoring, and Control of Operational Processes. School of Electrical and Computer Engineering, National Technical University of Athens, March 2024 https://www.didaktorika.gr/eadd/handle/10442/56130.
53. Jobert, M.; Wilson, F. J.; Ruigt, G. S. F.; Brunovsky, M.; Prichep, L. S.; Drinkenburg, W. H. I. M. Guidelines for the Recording and Evaluation of Pharmaco-EEG Data in Man: The International Pharmaco-EEG Society (IPEG). Neuropsychobiology 2012, 66(4), 201–220. https://doi.org/10.1159/000343478.
54. Alizadeh-Taheri, B.; Smith, R. L.; Knight, R. T. An Active, Microfabricated, Scalp Electrode-array For EEG Recording. In Proceeding of the International Solid-State Sensors and Actuators Conference - TRANSDUCERS '95. https://doi.org/10.1109/sensor.1995.717088.
55. Zhang, L.; Guo, X.; Wu, X.; Zhou, B. Low-cost circuit design of EEG signal acquisition for the brain-computer interface system. In Proceeding of 6th International Conference on Biomedical Engineering and Informatics, Dec. 2013. https://doi.org/10.1109/bmei.2013.6746942.
56. Analog Devices, Inc. AD8422: 1.8 nV/√Hz, Rail-to-Rail, Low Power Instrumentation Amplifier. Data Sheet. Available online: https://www.analog.com/media/en/technical-documentation/data-sheets/ad8422.pdf. (accessed on 10 Feb. 2024).
57. Zumbahlen, H. Analog Filters. Linear Circuit Design Handbook, H. Zumbahlen, Ed. Burlington: Newnes, 2008, 581–679. https://doi.org/10.1016/b978-0-7506-8703-4.00008-0.
58. Wang, J.; Tang, L.; E Bronlund, J. Surface EMG Signal Amplification and Filtering. International Journal of Computer Applications 2013, 82(1), 15–22. https://doi.org/10.5120/14079-2073.
59. Hsueh, J.-J.; Chen, T.-S.; Chen, J.-J., & Shaw, F.-Z. Neurofeedback training of EEG alpha rhythm enhances episodic and working memory. *Human Brain Mapping* **2016**, 37(7), 2662–2675. https://doi.org/10.1002/hbm.23201

 doi:10.20944/preprints202404.2023.v2

60. Texas Instruments, INA333 Low-Power, Precision Instrumentation Amplifier. Available online: https://www.ti.com/lit/ds/symlink/ina333.pdf (accessed on 12 Feb. 2024)